



## COMPOSITE MATERIAL MODELING FOR BLAST PROTECTION

Technical Final Report

MSC TFR 3705/CB02

March, 1997

Contract No. DAAB12-96-C-0013

Prepared by: Chian-Fong Yen and Mark L. Jones

For the period

May 2, 1996 to November 1, 1996

DISTRIBUTION STATEMENT A: Approved for Public Release

Distribution Unlimited - Mar 96

Prepared For:

Night Vision and Electronic Sensors Directorate

Countermeasure Division

10221 Burbeck Road

Fort Belvoir, VA 22060-5806

**DTIC QUALITY INSPECTED 2**

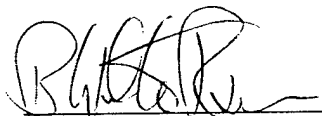
19980312 036

## PREFACE

This report contains the results of a SBIR Phase I program conducted at Materials Sciences Corporation under contract DAAB12-96-C-0013 from the U.S. Army, Fort Belvoir, under the sponsorship of the United States Marine Corps (USMC).

This effort was performed from May 2 through November 1, 1996. The Materials Sciences Corporation (MSC) Program Manager as Dr. Mark Jones, and the Principal Investigator was Dr. Chian-Fong Yen. The U.S. Army Technical Monitor was Dr. Stephen Souk of CECOM, who provided much assistance in guiding the program through to completion. The assistance of Messrs. Noel Wright and Jim Dillon of CECOM, Drs. Chris Hoppel and Fred Gregory of the Army Research Lab., and Mr. Richard Ellis of the Marine Corps is also gratefully acknowledged.

Approved by:

  
\_\_\_\_\_  
B. Walter Rosen, President

## TABLE OF CONTENTS

	Page
INTRODUCTION .....	1
PHASE I SUMMARY .....	3
PHASE I OBJECTIVE .....	5
DESCRIPTION OF TASKS AND RESULTS .....	6
TASK I - COMPOSITE MODELS .....	7
TASK II - BLAST LOAD ESTIMATION .....	11
TASK III - HYDROCODE ANALYSES .....	15
TASK IV - BLAST DAMAGE SIMULATIONS AND PARAMETRIC STUDIES....	23
CONCLUSIONS .....	25
REFERENCES .....	26
GLOSSARY .....	28
FIGURES .....	31
APPENDIX A. AN EQUATION OF STATE FOR TRANSVERSELY ISOTROPIC MATERIALS .....	A-1
APPENDIX B. A MIXTURE THEORY FOR EQUATION OF STATE.....	B-1
APPENDIX C. COMPOSITE LAYER FAILURE MODEL.....	C-1

## INTRODUCTION

The opportunity presented in this SBIR program is to develop models for composite material response of deformation and failure under mine blast conditions. Integration of these material models into a proven commercial hydrocode will significantly enhance the analytical capability in evaluating and designing lightweight composite material and structural concepts for the United States Marine Corps crew protection kits (CPK).

The USMC/USA has been successfully developing crew/vehicle protection kits (CPK) to provide increased crew survivability of tactical wheeled vehicles subject to mine blast [1-3]. However, these CPK's are currently based on a conventional steel/aluminum construction and are close to ½ ton in weight. As may be expected, there are payload and mobility penalties associated with the utilization of these devices in the field. Use of lightweight composite material elements presents an opportunity for significant weight savings.

Composite materials offer high strength and high stiffness at a fraction of the weight of competing metallic materials. However, they differ significantly in behavior from metallic materials especially in terms of their failure modes and energy absorption characteristics. All the major structural characteristics of the composite materials (strength, stiffness, failure mode, energy absorption) are dependent on the details of the composite construction. The problem is further complicated by the response of composite structures to high speed dynamic loading such as blast. Under blast loading conditions, shock waves are generated.

A composite laminate is usually composed of layers of fiber reinforced layers which are oriented in various directions. The stiffness and strength perpendicular to the fiber axis are usually much smaller than those parallel to the fibers. Thus, propagation of shock waves generated by blast loading becomes an anisotropic and multilayer problem requiring increased complexity. Under such complicated shock conditions, complex interactions occur between the layers and generate complex damage states involving delaminations and fiber damages.

It may be readily seen that efficient composite design requires an integrated approach whereby, the material selection, material construction, and response of the structure are all considered concurrently. In general, hydrocodes, however, have been developed mainly for isotropic structures. Phase I of this study has demonstrated that dynamic structural

analysis with the presence of shock waves can be accomplished by the integration of composite material models with a hydrocode. Further research efforts are needed to fully implement these composite material models with the hydrocode and validate the modeling capability for USMC composite structures.

The computer program chosen for further development is the hydrocode LS-DYNA3D. LS-DYNA3D is a three-dimensional, Lagrangian, finite element wave propagation computer code [4, 5]. Its capability of modeling problems of explosive loading, shock impact and its flexibility in adopting composite material models have been evaluated in the Phase I study. Though LS-DYNA3D will be used, the methodology developed in this SBIR research will be applicable to other hydrocodes. The development and capability of various hydrocodes are reviewed in [6, 7].

## PHASE I SUMMARY

Phase I accomplishments are summarized as follows:

1. Identification and development of the following missing elements for application of LS-DYNA for composite blast modeling

- Equation of state for heterogeneous anisotropic media
- 3D composite failure models

2. Demonstration of blast modeling of a composite sandwich panel

The capability of utilizing LS-DYNA3D to model the composite structural response under mine blast conditions have been critically evaluated. Figures 1 and 2 show the response of a simply supported sandwich plate subjected to transverse blast loading with due consideration to the progression of tensile fiber failures in the composite face sheets. The results have clearly demonstrated the unique capability of LS-DYNA3D in modeling progressive failure within composite structures. It is, however, necessary to enhance the modeling capability to accurately simulate the complicated failure behavior in blast loaded composite structures.

3. Identification of potential composite failure modes under mine blast conditions

In general the basic damage modes, which may occur in a composite structure subjected to impact loading, are matrix cracking, delamination and fiber breakage. The degree of interaction among these basic modes is strongly dependent on the impact conditions, structural configurations, and boundary constraints. Potential damage modes, which may be important to composite structures under blast loading conditions, have been evaluated utilizing LS-DYNA3D. These critical damage modes are:

- Delamination induced by in-plane shock wave, Figure 3.

- Through the thickness compressive failure and interply separation, Figure 4.
  - Fiber damage and matrix shear failure, Figure 1.
4. Integration of the 3D composite failure model within LS-DYNA3D for progressive failure identification

The MSC 3D composite failure model has been successfully incorporated into LS-DYNA3D through the user-defined material option. The failure model is applicable to thin shell element, thick shell element and 3D brick element. It allows the definition of the failure criteria of each layer in an arbitrary composite layup configuration within a shell element. Progression of various fiber and matrix failure modes within each layer are modeled during the dynamic analysis utilizing some simplified property reduction criteria. Figure 5 demonstrates the evolution of delamination failure in the face sheets of a sandwich panel subjected to mine blast loading. The progressive property degradation model will need further improvement in the Phase II study.

## PHASE I OBJECTIVE

The overall objective of this SBIR program was to develop an analytical method for evaluating alternate composite structural concepts for the USMC vehicle crew protection kit under mine blast conditions. The following were the specific objectives of the proposed Phase I effort:

1. Development of composite material behavior models suitable for the determination of composite deformation and failure under blast load.
2. Establishment of a blast load prediction capability within the proven commercial hydrocode LS-DYNA3D.
3. Improvement of the hydrocode LS-DYNA3D with integrated composite behavior models for blast structural analysis.

To meet these objectives, the work was divided into four tasks as described below:

### Task I - Composite Models For Hydrocode Analysis

Task Ia - Equations of State

Task Ib - Constitutive Relations

Task Ic - Failure Models

### Task II - Blast Load Estimation

### Task III - Hydrocode Analyses

Task IIIa - Hydrocode Evaluation

Task IIIb - Model Integration

Task IIIc - Code Demonstration

### Task IV - Parametric Studies

Descriptions of works performed in these tasks are given next.



## DESCRIPTION OF TASKS AND RESULTS

### **TASK I - COMPOSITE MODELS**

The objective of this task is to evaluate and develop simple material models for dynamic analysis of composite materials for the mine blast load conditions. Development of appropriate composite material models requires three sub-tasks to be addressed: (1) equation of states are required to determine the composite level shock response under blast conditions; (2) constitutive relations are required to translate composite level loads into fiber and matrix stresses and strains; and (3) failure models are required whereby these local material stresses may be compared with local material strengths for damage assessment.

An equation of state that is suitable for a transversely isotropic medium has been derived. The equation of state is generalized to include the portion of pressure resulting from the deviatoric strain which is neglected in LS-DYNA3D, since it does not exist for isotropic material.

A micromechanics based equation of state for a unidirectional composite layer has been developed utilizing a simple mixture approach. The effective equation of state accounts for the composite compressibility effects (change of density) and the irreversible thermodynamic processes (such as shock heat) based on the corresponding shock properties of the fibers and the matrix.

A layer failure model based on the 3D failure criteria of Hashin [8] with a slight modification have been provided. Also provided is a generalized Coulomb-Mohr failure criterion, which may be able to better characterize the composite matrix failure mode under compression dominated loads [9].

#### Task Ia - Equations of State

Current hydrocode modeling capabilities for shock behavior are confined almost exclusively to isotropic homogeneous media. Little provision has been made for anisotropic heterogeneous composite materials. Propagation of shock waves through these media produced by blast impact may result in many complex phenomena associated with direction-

ally dependent material properties, strength and failure mechanisms. Before accurate predictions of composite failure under shock waves can be achieved, the behavior of constituent materials under the shock state and the associated release path must first be understood.

Generalization of a hydrocode for anisotropic composite materials requires consideration of two elements:

- 1). Appropriate constitutive relations to account correctly for anisotropic effects.
- and
- 2). A procedure whereby shock effects are partitioned within the constituents.

Within the general framework of a hydrocode, a constitutive relation describes the particular nature of the material by relating the stress in the material with the amount of distortion (strain) required to produce this stress; and an equation of state relates the density (or volume) and internal energy (or temperature) of the material with pressure. While current commercial hydrocodes such as DYNA3D have successfully incorporated anisotropic constitutive models, further effort is required to generalize the equation of state for fully anisotropic materials. An additional procedure is also required whereby the shock effects are effectively partitioned between the fibers and the matrix. To accomplish these generalizations, two subtasks are required.

#### Anisotropy Generalization

In an isotropic medium, application of hydrostatic pressure will produce a uniform strain. However, for a general anisotropic body, a hydrostatic pressure will introduce different normal strain components in the three principal directions. Therefore, for anisotropic materials, application of pressure produces both a volumetric strain (dilatation) and a deviatoric strain. Since shock wave experiments on isotropic materials typically provide data for the pressure as a function of volumetric strain, a consistent procedure has to be developed to interpret the high-pressure material response (equation of state) so that the summation of the deviatoric stresses and the thermodynamic pressure will provide the correct stresses in the elastic regime.

An equation of state that is suitable for a transversely isotropic medium has been derived. The results are given in Appendix A. The equation of state is generalized to include the portion of pressure resulting from deviatoric strain. This formulation has been established to minimize the necessary modification of the hydrocode LS-DYNA3D in order to implement the anisotropic generalization. This is because in LS-DYNA3D, the total stress is separated into deviatoric stresses and thermodynamic pressure which is a formulation commonly used in classical plasticity theories. Integration of these more general equations of state in the LS-DYNA3D code will be performed in Phase II.

### A Mixture Theory

In the capacity of current hydrocodes, a composite material can be modeled by a given number of orthotropic homogeneous layers of different orientations. This requires the knowledge of the effective shock properties for a composite layer before the start of the analysis. In this Phase I, a simple mixture approach similar to that given by Torvik [10] is used to develop a micromechanics based equation of state for a unidirectional composite layer. The effective equation of state accounts for the composite compressibility effects (change of density) and the irreversible thermodynamic processes (such as shock heat) based on the corresponding shock properties of the fibers and matrix. This provides a simple but effective micromechanical approach for partitioning the composite shock properties and incorporate it in the macroscopic hydrocode LS-DYNA3D for shock wave analysis. The derivation is given in Appendix B.

It is known that the shock responses of fibers and matrix are, in general, very different; typically, the matrix material is considerably more compliant than the fiber. The passage of a shock wave will result in different thermodynamic states for the two materials. Therefore, it is necessary to obtain a more accurate thermodynamic material response of a composite layer by using the dynamic material characteristics of each constituent at every time step.

In Phase II the mixture theory will be used to treat the individual thermodynamic responses of a composite material within the context of a macroscopic continuum computer code. The methodology will be complex enough to encompass the essential physics, and yet sufficiently simple for incorporation into existing hydrocodes.

The requirements for incorporating a mixture theory within a hydrocode has been discussed in [11, 12]. In general, alterations to the mass and momentum conservation equations in hydrocodes to characterize the dynamic response in each constituent is a formidable task. On the other hand, constitutive equations and the energy equation are relatively easy to access and modify. Thus, a simple mixture theory may be formulated by considering no relative motion between the constituents. At each time increment computation, the position, velocity and acceleration of a basic composite mixture will be obtained on the homogenous macroscopic element level. The thermodynamic variables in individual constituents including density, pressure, temperature and internal energy will then be computed on the microscopic level. The micromechanical formulation of the mixture theory is based on the equations of state and energy equations of each constituent together with the definition of volume fraction mixture of the constituents. A subcycling numerical scheme based on the mixture theory will be developed and incorporated into the hydrocode LS-DYNA3D.

#### Task 1c - Failure Models

The failure analysis capability for laminated composites provided by the hydrocode LS-DYNA3D has been examined. The model for layer failure used in LS-DYNA3D is the Chang-Chang model, [13], which provides various failure modes solely due to in-plane stresses in a unidirectional layer. In this 2D failure model, the failure modes due to out-of-plane shear and through the thickness normal stresses are neglected. It is, however, known that all the six stress components can be generated when a laminate structure is subjected to transverse blast loading and can play significant roles on layer failure. In addition to the in-plane failure modes, crash failure may result due to the high blast pressure load. Shear failures in the layers may result due to the high out-of-plane shear stresses. Furthermore, it is known that delamination in laminated composite plates is significantly influenced by out-of-plane shear stresses.

A layer failure criterion based on 3D stresses with improved failure modeling capability for the current application is provided in Appendix C. This failure model was incorporated in LS-DYNA3D in this Phase I study. This 3D failure model was encoded as a user-defined subroutine for the use in LS-DYNA3D. This material subroutine was successfully compiled

and linked with LS-DYNA3D on a Pentium-based PC. Assistance was provided by KBS2 Inc., which is the vender of the current PC version of LS-DYNA3D, to accomplish this task. Results utilizing the material model for failure identification within LS-DYNA3D are reported in Task IV.

In this work a Coulomb-Mohr failure criterion was also evaluated for its applicability to characterize the composite matrix failure mode under compression dominated loads. This capability is essential for mine blast applications, since when a composite plate is subjected to transverse blast loading, high compressive waves propagating through the thickness of the plate can be generated.

According to Hashin's arguments [8], high compressive stresses applied in the direction transverse to the fibers can result in matrix mode compressive failures. Note that matrix failures must occur without fiber failure and hence they will occur on planes parallel to fibers. Hashin suggested matrix failures in tensile and compressive modes based on the property of transverse isotropy of a ply and other physical arguments. While the tensile failure criterion can characterize experimental data reasonably well, the compressive failure criterion is not well tested especially in the high pressure region. Recently, at MSC, a matrix mode failure model based on a generalized Coulomb-Mohr type criterion has been successfully utilized to correlate some failure data for high compressive loads, [9]. By considering only the effect of the two normal stresses  $\sigma_2$  and  $\sigma_3$  that are transverse to the fiber direction, the failure surface based on the Coulomb postulate has the form

$$\begin{aligned}\sigma_3 &= -\sigma_T + m\sigma_2 \\ m &= (1 + \sin \phi) / (1 - \sin \phi)\end{aligned}\tag{1}$$

where  $\sigma_T$  is the uniaxial transverse compressive strength and  $\phi$  is the inclination of the planes of fracture. Note that  $\sigma_T$  and  $\phi$  can be measured from a transverse compression test.

Failure surfaces of Hashin and Coulomb-Mohr criterion are compared in Figure 6 utilizing the experimental data provided by Collings [14]. The transverse compressive strength is 120 MPa and  $\phi = 40^\circ$ . As shown in Figure 6, compression cut-offs based on maximum shear stress are provided at very high compressive stresses. This is due to the fact that at the very high pressure region, the compressive failure transfers from the matrix compression mode to a fiber shear failure mode [14]. Because of the presence of fibers, stresses

to cause such fiber shear failures are extremely high, and may be much higher than the maximum compressive stresses under the current mine blast conditions.

It is seen from Figure 6 that the discrepancy between these two criteria increases as the stress increases. When a composite plate subjected to a transverse blast of 3000ATM (304 MPa) peak pressure, the contact stress is  $\sigma_3 = 304$  MPa. However, under the blast loading, high in-plane transverse stress  $\sigma_2$  is usually caused due to the resistance to Poisson's strain. It is seen from the failure surfaces of Figure 6, the composite plate would fail with the existence of  $\sigma_2 > -120$  MPa for the Hashin failure surface and  $\sigma_2 > -40$  MPa based on the Coulomb-Mohr surface.

The compressive stresses occurring in a blast-loaded plate can be very complicated. The high through the thickness compressive wave can interact with the flexural compressive wave propagating in the plane of the plate. The compressive stresses under mine blast conditions are likely to be in the range of 100 MPa to 400 MPa. In Phase II, the applicability of both the Hashin's and the Coulomb-Mohr type compressive failure criteria in the region of concern will be further evaluated by correlation with published experimental data.

## **TASK II - BLAST LOAD ESTIMATION**

Description of blast wave formation and the effects of blast loading on structures may be found in numerous references, e.g., [15]. In general, when a quantity of high explosive material is caused to detonate in air, the hot highly compressed gaseous products of the reaction act on the air surrounding the explosive, rapidly forcing it out of the volume it occupied. This causes a shock wave to propagate in the air with an instantaneous high pressure pulse propagating along the wave front. Precise analysis of 3D blast waves and blast wave effects can be very time consuming.

The purpose of performing mine-blast wave analysis for a CPK structure is twofold. First, the analysis will provide the blast loading history for structural integrity evaluation. Second, it will provide the evaluation of blast wave deflection capability of the CPK structure. There are three possible approaches reported in the literature for blast wave interactions: (1) simple analytical blast models, (2) hydrocode analysis with proper equation of

state for the compressed air, and (3) use of detailed CFD codes such as AUGUST code developed by SAIC [1-3]. Evaluation of these approaches were performed in Phase I.

#### (1) Simple Analytical Blast Model

For dynamic analysis of structures, the blast effects are most conveniently represented by a loading-time history that is applied to the structural member as transient loading. The pressure-time history of a typical blast wave as observed at a location reasonably removed from the center of explosion is shown in Figure 7. At an arrival time (e.g.,  $t=0$ ) after the explosion, the pressure at this location rises quickly to a peak value of overpressure above the local ambient pressure,  $P_0$ . The pressure then decays to ambient in time  $t_s$ , to a partial vacuum of very small amplitude, and eventually returns to  $P_0$ .

#### Incident Overpressure

Defining the form of the wave decay in a mathematical form is not a simple task. Expressions of varying complexity have been suggested by some investigators as cited in [16]. However, a most commonly used form is that the decay overpressure is described as quasi-exponential in character. In terms of a dimensionless wave form parameter  $\alpha$  and time  $t'$  measured from the instant the shock front arrives, the relation is established as

$$\begin{aligned} t_p \geq t \geq 0 \quad P(t) &= \frac{t}{t_p} P_s \\ t \geq t_p \quad P(t) &= (1 - t') e^{-\alpha t'} P_s, \quad t' = \frac{t - t_p}{t_s - t_p} \end{aligned} \quad (2)$$

It is noted that the loading-time relation at a certain location is characterized by the values of the rise time  $t_p$ , the duration time for the shock wave  $t_s$ , the decay parameter  $\alpha$ , and the peak overpressure  $P_s$ . For a certain type of explosion, these parameters are usually expressed in terms of the distance from the center of explosion to the given location,  $R$ , and the weight of explosive,  $W$ . Various expressions such as  $P_s = P_s(R, W)$  have been given in literature for various explosions ranging from conventional high explosives to atomic weapons, e.g., [15].

### Reflected Overpressure

Although blast loading may also be affected with the airflow behind the shock front, it is known that the most destructive effect of a blast wave is usually by the peak over pressure under blast conditions. When the blast reaches a rigid object at right angle, the resulting reflection produces a reflected overpressure,  $P_r$ , which is simply given by

$$P_r = 2P \quad (3)$$

where  $P$  is the incident overpressure given by equation (2). This perfect reflection assumption will always yield high estimates of reflected impulse.

During the Phase I study, it has been recognized that LS-DYNA3D incorporates a simple analytical blast model to provide blast pressure history on structure surfaces. It is also recognized that the computer code ConWep, used by the ARMY [17], also provides reflected pressure histories under air blast conditions. Utilizing an equation similar to equation (2), ConWep provides the parameters of pressure decay for the explosion of a wide variety of weapons.

#### (2) Hydrocode Analysis

It is seen from the literature that hydrocodes have been used for the simulation of blast wave interactions with structures [18, 19]. Good correlation between hydrocode results and experiments have been reported. In general, a hydrocode has the potential to be an efficient tool for the detailed investigation of complex blast wave propagation problems by including some basic capabilities such as (1) grid remapping function, (2) Euler grid formulation, and (3) selection of various equations of state. Typical procedures for blast simulation provided in [18] are described in the following paragraphs.

Euler remapping capability is essential for blast loading problems. Blast problems are usually represented by means of an Euler grid in which material is transported from one cell of the grid to another. The grid remains fixed in space and undeformed in contrast to a Lagrangian grid which does deform and through which material is not transported. The latter grid formation is known to be more suitable for structural analysis. The blast analysis involves establishing a fine, wedge-shaped grid at the apex of which the explosive material



(TNT) is located. In this case, a calculation is usually run as a one-dimensional (1D) grid until a reflecting surface is encountered by the blast wave when a 2D or 3D grid is created and filled by the remapping facility.

The TNT is commonly modeled by the so-called JWL equations of state (EOS) [4]. When a JWL has expanded to more than a certain amount (e.g., 10 times) of its original volume, the EOS can be converted to that of an ideal gas as described in [18]. Consequently, TNT is modeled as an ideal gas in the converted 2D or 3D grid. Through proper selection of grid size, EOS and integration time step, good correlation with experimental measurements can be achieved for some complex blast/structure interaction problems.

The blast wave modeling capability has recently been installed in LS-DYNA (version 940) [20] provided by Livermore Software Technology Corporation [21]. Figure 8a shows a 3D Eulerian problem of a one quad of cylindrical shell, with high explosive Eulerian mesh inside the cylinder, and Eulerian air mesh outside the cylinder. Figure 8b shows the initial and final geometry of the cylinder. Figures 9a and 9b show the velocity and displacement time history of a node at 2.54 cm from the detonation point, respectively. While it is obvious that LS-DYNA is capable of modeling simple blast wave problems, it is necessary to further evaluate this capability and assess the accuracy of this approach for modeling complex blast wave problems such as those for CPK design.

### (3) CFD Code Analysis

Computational fluid dynamic (CFD) simulations were performed for CPK structures at SAIC by using the AUGUST code [1-3]. In this code, the second order Godunov method was used on adaptive unstructured tetrahedral grids while the Becker-Kistiakowsky-Wilson (BKW) equation of state was used for accurate simulation of the initial phase of blast expansion [3].

AUGUST adapts the unstructured grid system which is very well suited to implement the boundary conditions on complex geometrical shapes such as those for a military cargo truck. It also provides a grid generating scheme which allows the capacity of grid refinement and coarsening based on the local shock wave conditions. This code has been successfully applied to predict the pressure distribution due to mine blast and CPK interaction at close range.

The AUGUST code, however, does not provide a direct link to dynamic structural analysis codes for damage analysis of structures subjected to blast loading conditions. Furthermore, this code currently is not in the public domain and may not be available for potential designers of applications such as CPK.

It appears that the simple blast model can provide some reasonable estimates for mine blast pressure histories. Computer codes such as ConWep can be readily used to perform preliminary evaluation of various material and structural concepts for enhancing mine blast resistance. It is believed that the AUGUST code can provide the most accurate shock pressure prediction for performing detailed CPK design. It would be desirable for a designer to be able to access the AUGUST code directly for various Phase III applications of this SBIR project. The emerging capability of analyzing blast wave in air and its interaction with a target structure adopted in some commercially available hydrocodes provide other alternatives for blast load estimation. It, however, requires further evaluation with regards to the accuracy in predicting the shock pressure histories for mine blast and structure interaction in close range.

### **TASK III - HYDROCODE ANALYSES**

#### **Task IIIa - Hydrocode Evaluation**

The capabilities of LS-DYNA3D were evaluated by performing mine blast analysis of a wide variety of composite plates and shells. Results of this evaluation task performed are summarized as follows.

#### **Element Selection**

Three types of elements were evaluated including (i) shell, (ii) thick shell, and (iii) 3D continuum. The results are summarized in Table 1. It is seen from Table 1 that both shell and thick shell elements provide the capability for user-defined laminate layup. However, only the thick shell formulation is consistent with the 3D stress representation which is essential for application of the 3D failure model. Consequently, the thick shell element is

most suited for the use of modeling dynamic behaviors of composite structures under mine blast conditions.

Table 1. A Comparison of the Feature of the Current LS-DYNA Composite Elements

Element Type	Analysis Requirements				
	Laminate Input	3D Stress	Lamina Failure *	Post Processing	Composite Equation of State
Thin Shell	Yes	No	2D	Yes	No
Thick Shell	Yes	Yes	2D	No**	No
3D Brick	No	Yes	2D	Yes	No

\* Indicates a 3D failure model is required

\*\* Indicates an improved version is required

#### Failure Model

As described in the Task Ic subsection, the current LS-DYNA3D composite laminate failure analysis model considers only a 2D stress state for composite laminates. Once failure occurs in a composite layer, the material may undergo some degree of property loss in the damaged area. The degree of property loss are strongly dependent upon the failure mechanisms resulting from the damage. Consequently, the material degradation model is usually established on the basis of the proposed failure criterion. Due to the use of a 2D failure criterion, the progressive damage analysis capability provided by LS-DYNA3D is again limited to in-plane fiber and matrix damages. In Phase I of the research, a 3D failure criterion has been successfully incorporated into LS-DYNA3D. As provided in Appendix C, the 3D failure criterion accounts for five basic failure modes in a unidirectional layer including (1) fiber tensile mode, (2) fiber compressive mode, (3) matrix tensile mode, (4) matrix compressive mode, (5) delamination mode. These failure modes are represented by five distinct failure functions. The 3D criterion used in this study enhances the simulation capability of LS-DYNA3D.

Simple property degradation procedures have been adopted in the user-defined subroutine described in Task Ic. When fiber tensile and compressive failures are predicted in a

composite layer, the layer is assumed to carry no load. When a layer delamination condition is satisfied, the layer is assumed to carry no tensile load through the thickness. The effect of matrix damage on the layer stiffness is neglected. It should be noted that these property reduction criteria are oversimplified for the sake of easy incorporation in LS-DYNA3D for the Phase I damage evaluation. Some preliminary results of progressive failure analysis are presented later in the subtask IIIc. It is recommended that in the Phase II study, some fracture mechanics based property degradation criteria be investigated to better characterize the progressive damage states in composite structures under mine blast conditions.

#### Material Model and Equation of State

LS-DYNA3D includes a group of constitutive laws and equations of state for a wide variety of materials. However, input properties for LS-DYNA3D analysis are limited to single phase materials including that for a composite layer. For composite applications, stand-alone computer codes have been developed at MSC to evaluate effective layer properties (including progressive damages) from constituent properties based on some well developed micromechanical models. These material models have been integrated with the commercial finite element code ABAQUS [23, 24] for use in general structural analysis. Such material analysis codes can also be incorporated into LS-DYNA3D through the user-defined material subroutine. However, it would be more convenient to establish a preprocessing procedure for the constituent property input and the effective composite property calculation.

Implementation of the micromechanics based equation of state suitable for a transversely isotropic composite layer developed in Task Ia requires modification of the source code at both the preprocessing and the computation levels. Attempts to implement the material analysis model and the composite equations of state will be explored in Phase II.

#### Pre- and Post-Processing

MSC had contacted KBS2 Inc. at Burr Ridge, IL, which is the vendor of the current PC version of LS-DYNA3D, concerning the post processing capability. In responding to the

need for this SBIR research, KBS2 provided MSC with an improved version to support the post processing for the thick shell element.

Additional enhancements are needed for pre- and post-processors capability within LS-DYNA3D to fully accommodate composite material inputs and evaluation of composite blast response. These include:

- Input for constituent properties and composite layup configurations.
- Procedures for blast loading application.
- Visualization of the progression of composite failure development for selected modes.

Such enhancements will be accomplished in Phase II.

### **Task IIIc - Code Demonstration**

LS-DYNA3D was used to analyze a simply supported sandwich plate subjected to transverse blast loading with due consideration to tensile fiber failure in the composite face sheets. This code was also used to identify various potential failure modes, which may occur in composite structures under blast loading conditions. The results are presented as follows.

#### **(1) Fiber Failure in a blast loaded sandwich panel**

A typical pressure-time history of a mine blast wave was used to perform the mine blast simulations. The peak overpressure was at 1390ATM (141 MPa, 20.4 ksi) with an assumed rising time of 0.1  $\mu$ -sec. The pressure was assumed to decay exponentially after the peak load. Note that for simplicity this simple pressure-time history has been used for the Phase I demonstration. More accurate pressure history pulses can be obtained from the codes such as AUGUST [1-3] and ConWep [17].

A 164cm x 164cm simply supported composite sandwich plate was considered. The top 7.1mm-thick face and the bottom 9.7mm-thick face consisted of ply layups of symmetric and quasi-isotropic [0/90/ $\pm$ 45]<sub>ns</sub> configurations. The syntactic foam core layer had a thickness of 27.6mm. The elastic properties for a transversely isotropic unidirectional

S2/Epoxy layer shown in Table 2 are:  $E_A = 55.9\text{GPa}$  (8.1 Msi),  $E_T = 18\text{GPa}$  (2.6 Msi),  $\nu_A = \nu_T = 0.27$ ,  $G_A = 7.6\text{GPa}$  (1.1 Msi). The isotropic elastic properties of the syntactic foam core are  $E = 2.21\text{GPa}$ ,  $\nu = 0.35$ , [22]. The densities for the face sheet and the core materials are 1.99g/cc and 0.721g/cc, respectively.

The finite element model consisted of a  $\frac{1}{4}$ -symmetry coarse mesh of 400 thick plate 8-noded elements. Both the face sheets had one through the thickness element, while the core had two thickness elements. Only one quadrant of the square sandwich panel was modeled because of the geometric symmetry and the effective quasi-isotropic composite properties. The nodes on the outer edges of the bottom face sheet were fixed in the z-direction to simulate simply supported conditions. The symmetry edges of the model were constrained according to the symmetry about xz and yz planes. The pressure pulse was applied uniformly to the top surfaces of each of the top face elements.

LS-DYNA3D allows definition of an arbitrary composite layup configuration within a shell element. Each ply in the layup configuration has a unique orientation angle which measures the offset from some reference in the element. Each integration point through the shell thickness (typically though not limited to one point per ply) requires the definition of the ply orientation angle at that point. In each element of the top and bottom face sheets, 16 layers with  $[0/90/\pm 45]_{2s}$  layup were specified for the blast analysis.

The model for layer failure used in LS-DYNA3D is the Chang-Chang model, [13], which provides various failure modes solely due to in-plane stresses in a composite layer. One of the most dominant failure modes due to in-plane loading is the fiber failure. In this task, this 2D failure model was used to simulate the panel deformation with the progression of ply-by-ply fiber failure under the blast loading condition. Due to the limitation of this failure model, only the tensile fiber failure mode was considered. Nevertheless, the following results will clearly demonstrate the unique potential of utilizing LS-DYNA3D to model the dynamic composite response with due consideration to progression of various failure modes.

Table 1. Material Properties Used for Dynamic Analysis

Material	Elastic Properties					Composite Strengths							Fracture Properties	Density
	E <sub>a</sub> GPa (Msi)	E <sub>t</sub> GPa (Msi)	ν <sub>a</sub>	ν <sub>t</sub>	G <sub>a</sub> GPa (Msi)	S <sub>1</sub> <sup>t</sup> GPa (ksi)	S <sub>1</sub> <sup>c</sup> GPa (ksi)	S <sub>2</sub> <sup>t</sup> GPa (ksi)	S <sub>2</sub> <sup>c</sup> GPa (ksi)	S <sub>12</sub> GPa (ksi)	S <sub>23</sub> GPa (ksi)			
IM7/8552	158.6	11.5	0.311	0.35	5.0	2.72	1.69	0.111	0.305	0.12	0.176	300	1.6	
	(23)	(1.7)			(0.73)	(395)	(245)	(16.1)	(44.2)	(17.4)	(25.5)		(1.49x10 <sup>-4</sup> )	
S2/3501-6	55.9	18	0.27	0.27	7.6	1.79	0.96	0.06	0.16	0.11	0.083	160	1.99	
	8.1	(2.6)			(1.1)	(260)	(140)	(9.0)	(22.5)	(16.0)	(12.0)		(1.86x10 <sup>-4</sup> )	

The blast pressure pulse was applied normally on the top face of the sandwich plate. Plots of panel deformation and stress contours of the in-plane normal stress in the x direction,  $\sigma_x$ , at 0.5msec, 1.0msec, 1.5msec and 2.0msec are shown in Figures 10-13. It is seen from Figure 12 (at 1.5msec) a tensile peak stress of about 240 ksi occurred in the element at the center bottom face sheet. The element eventually failed due to the progression of fiber failures in all the composite layers in this element. Note that the ply has an axial tensile strength of 260 ksi. Figure 13 shows that at 2.0msec, the failed element was eliminated from the model, and load redistribution was computed. The progression of damage due to the tensile fiber failure mode is more clearly demonstrated by the stress plots of the bottom face sheet as shown in Figures 14 to 17.

The above analysis results clearly demonstrate the capability of LS-DYNA3D in modeling the progressive failure of a composite structure. However, it should be noted that it is necessary to enhance its damage modeling capability for other important failure modes. In addition to fiber failure mode, other potential failure modes, which may occur in composite structures under blast loading conditions, are identified in the following subsections.

## **(2) Delamination induced by in-plane shock wave**

Delamination may result as shock waves propagating in a composite laminate. As a shock moving in the plane of a laminated plate, shock waves will propagate with different velocities in differently oriented layers. With the existence of bonded ply interfaces, the wave front of a faster wave will be pulled back while the slower wave will be pushed forward. This type of interaction introduces shear stress in the ply interfaces along the wave direction. Analyses results provided below indicate that such interface shear stresses near the shock wave front can be high enough to cause interply separation.

Computations were made to simulate a composite plate of infinite extent in the y-z plane that impacts a smooth rigid surface at  $x = 0$ . The composite plate consisted of  $[0/90]_n$  S2/Epoxy layers with x and y in the  $0^\circ$  and  $90^\circ$  directions, respectively.

Only a repeating layer,  $[0/90]_{1/2}$ , was modeled. Nodes were restrained in the y-z plane to give the proper lateral restraint to the model. Impact was simulated by giving all elements a uniform velocity of -25.4m/sec in the x-direction. This model was established to examine the potential damage behavior from shock wave moving in a composite laminate.



The results of normal stress  $\sigma_x$  and shear stress  $\sigma_{xz}$  at 0.2 $\mu$ -sec after the impact are shown in Figure 18. It is clearly seen in Figure 18a that the wave front in the 0-layer traveled much faster than that in the 90-layer. The wave front interaction between these layers resulted in high interlayer shear stress as shown in Figure 18b. It is noted that such shearing stresses are important near the shock front and near the layer interface. The shear stresses vanish at the center lines of each layer.

As the S2/Epoxy material was subjected to the impact velocity of 25.4m/sec, the peak axial stress in the 0-layer was 600 MPa (87 ksi) which is well below the allowable composite axial compressive strength of 960 MPa (140 ksi). However, the maximum shear stress of 78 MPa (11.3 ksi) reached the composite shear strength of 83 MPa (12 ksi). The likelihood of shear failure due to the propagation of in-plane shock waves is obvious.

### **(3) Through the thickness compressive failure and spall fracture**

Compressive failure and spall fracture may result as blast shock waves propagate through the thickness of a laminate plate. When a composite plate is subjected to a transverse blast load, a high compressive shock wave propagates through the thickness of the plate immediately after impact. After reaching the opposite free surface of the plate, the compressive wave is transformed into a reflected tensile wave. While compressive failure may result due to the high blast pressure, the reflected tensile wave may cause interply separation.

A fixed ended sandwich plate subjected to blast loading was analyzed. The fixed ended sandwich plate had a span of 164cm (66 in.) in the x direction and an infinite extent in the y direction. It has the same through the thickness configuration as that analyzed in subsection (1). The composite layup in the face sheet was [0/90/90/0]. The pre-processor within LS-DYNA3D was used to generate the FEM model for 1/2 of the plate. 8-noded brick elements were used. Fine mesh was established to accurately predict the through the thickness stresses. Nodes were restrained in the y-z plane to give the proper lateral restraint to the mode. The blast load which peaked at 1390ATM (141 MPa, 20.4 ksi) was applied normally on the center half of the top face of the sandwich panel.

Figures 19-22 show the shock waves of  $\sigma_z$  propagating through the thickness of the sandwich plate. High shock stress  $\sigma_z$  of 141 MPa (20.4 ksi) was directly from the contact

of the blast load. There was also a high in-plane transverse stress  $\sigma_y$  of 116 MPa (16.7 ksi) resulting from the resistance to Poisson strain. To identify the ply failure under such high pressure state required the use of the compressive matrix failure criteria discussed in Task Ic.

When the initial shock wave reached the opposite free surface of the plate, the compressive wave reflected into a tensile wave. After several reflections, a maximum tensile stress of over 75 MPa (11 ksi) was developed in some plies in the bottom face sheet, Figure 22. Due to a tensile transverse strength of 60 MPa (9 ksi) for the S2/Epoxy composite, the tensile wave may cause interply separation in the bottom face sheet. Further propagation of such a through the thickness failure may cause complete layer delamination or result in spall fracture.

In general, impact damage of a composite structure subjected to blast loading is a combination of matrix cracking, delamination and fiber breakage. The degree of interaction among these basic modes is strongly dependent on the impact conditions, structural configurations and boundary constraints. The examples given above clearly demonstrate that it is necessary to improve the composite failure analysis capability available in the current version of LS-DYNA3D to make it a useful design tool for composite structures under blast loading. Preliminary results of blast damage simulation utilizing LS-DYNA3D integrated with the MSC 3D failure model are presented in the next task.

#### **TASK IV - BLAST DAMAGE SIMULATIONS AND PARAMETRIC STUDIES**

The sandwich panel shown in Figure 9 was analyzed. The 3D failure model, together with the property degradation model described previously in Task Ic and Task IIIa, were used for simulation. For simplicity, only the fiber failure and delamination in the composite face sheets were considered, and the composite matrix failure and core failure were neglected. The layer elastic properties together with the strengths for the S2/Epoxy and IM7/8552 systems are listed in Table 2.

Plots of the deformed sandwich panel with S2/Epoxy face sheets at 0.5msec, 1.0msec, 1.5msec, 2.0msec, and 2.45msec are shown in Figures 23-27, respectively. From these figures one can observe the evolution of delamination in both face sheets due

to the propagation of the through the thickness shock waves and the subsequent flexural waves. As a reference, Figure 28 shows a photograph of a quadrant of a damaged square sandwich panel following a mine blast test. The blast test was performed by the Army Research Laboratory [22]. Note that the current analyses utilized the same sandwich configuration and materials. It is evident that the extensive delamination shown in Figure 27 can be qualitatively correlated to the test result of Figure 28.

Blast analyses of the sandwich panel were also performed to evaluate the effect of using IM7/8552 face sheets. It is seen from Table 2 that the IM7/8552 provides higher values of the transverse normal and shear strengths than the S2/Epoxy system. The IM7/8552 is known to provide improvement of delamination resistance for composite plates subjected to low energy impact conditions. Figures 29-31 show the deformation of the sandwich panel at 0.5msec, 1.0msec and 1.63msec, respectively. Despite the improved through the thickness strengths, extensive delamination is predicted in the IM7/8552 face sheets. In fact the spalling delamination in the bottom IM7/8552 face sheets is more pronounced than that in the S2/Epoxy face sheet at about 1.5msec. This is likely due to the fact that the high in-plane stiffness of the IM7/8552 system provides high bending resistance and results in high local delamination stresses.

## CONCLUSIONS

The Phase I program has been successful in demonstrating the integration of MSC's composite material models into the dynamic analysis code LS-DYNA3D for predicting deformation and failure of composite structures under mine blast conditions. The availability of such a dynamic analysis code for the design of composite structures under complex loading conditions will greatly facilitate the development of light weight composite CPKs.

The dynamic analysis code LS-DYNA3D was selected as the vehicle for further development. The selection is based on its capability to model explosive loading, shock and high velocity impact problems. Key accomplishments of the Phase I program are:

- Derivation equations of state for general heterogeneous anisotropic media that are suitable for composite shock wave analysis.
- Successful integration of first order MSC composite material models into LS-DYNA3D.
- Demonstration of this capability by analysis of a composite sandwich panel under blast loading conditions.
- Demonstration of the potential for performing progressive failure predictions through the implementation of a 3D failure model and the associated simple property degradation model.
- Identification of improved failure criteria that can better characterize the failure modes expected in composite structures under mine blast conditions

It should be noted that, though LS-DYNA3D was selected for this SBIR, the models and methods are generally applicable to other hydrocodes with user-defined material modeling capabilities.

## REFERENCES

1. Eidelman, S., Lottati, I. and Yang X., Development of Mine-Resistant Vehicles, SAIC Report 93/1141, Army Contract No. DAAL02-90-C-0071, July 1993.
2. Lottati, I. and Eidelman, S., Blast and Structural Simulation/Analysis for Development of a Centerline Blast Deflector for The Cab of An M923a2, 5-Ton Cargo Truck, SAIC Final Report, Contract No. DAAK70-94-U-0009, May, 1994.
3. Lottati, I., Dillon, J., Sergi S., Strittmatter, K., Sousk, S., and Eidelman, S., "Use of CFD/CSD Capability for Design of Blast Deflectors for a Mine Resistant Vehicle," Proceedings Military Applications of Blast and Shock, MABS-14, Las Cruces, New Mexico, September 1995.
4. "LS-DYNA3D User's Manual (Nonlinear Dynamic Analysis of Structures in Three Dimensions)," Version 936, Livermore Software Tech. Corp., August 1995.
5. Hallquist, J.O., "LS-DYNA3D Theoretical Manual," Livermore Software Tech. Corp., Rev. 2, July 1993.
6. Anderson, C.E., Jr., "An Overview of The Theory of Hydrocodes," Int. J. Impact Engnr, Vol. 5, pp. 33-59, 1987.
7. Johnson, W.E., and Anderson, C.E., Jr., "History and Application of Hydrocodes in Hypervelocity Impact," Int. J. Impact Engnr, Vol. 5, pp. 423-439, 1987
8. Hashin, A., "Failure Criteria for Unidirectional Fiber Composites," J. of Applied Mechanics, Vol. 47, 1980, pp. 329 - 334.
9. Chatterjee, S.N., "A Coulomb-Mohr Type Criterion for Matrix Mode Failure in a Lamina," presented at 13<sup>th</sup> Symposium on Composite Materials: Test and Design, May 1996.
10. Torvik, P.J., "A Simple Theory for Shock Propagation in Homogeneous Mixtures", Air Force Inst. Technology, WPAFB, OH, AFIT-TR-70-3, May 1970.
11. Drumheller, D.S., "Hypervelocity Impact of Mixtures," Int. J. Impact Engnr, Vol. 5, 1987, pp. 33-59.
12. Anderson, C.E., Jr., O'Donoghue, P.E. and Skerhut, D., "A Mixture Theory Approach for the Shock Response of Composite Materials," J. of Composite Materials, Vol. 24, 1990, pp. 1159-1176.

13. Chang, F.K., and Chang, K.Y., "A Progressive Damage Model for Laminated Composites Containing Stress Concentration," J. of Composite Materials, Vol. 21, 1987, pp. 834-855.
14. Collings, T.A., "Transverse Compressive Behavior of Unidirectional Carbon Fiber Reinforced Plastics," Composites, Vol. 5, 1974, pp. 108-116.
15. Beshara, F.B.A., "Modelling of Blast Loading on a Aboveground Structures - I. General Phenomenology and External Blast," Computer & Structures, V51, pp. 585-596, 1994.
16. Baker, W.E., "Explosions in Air," University of Texas Press, Austin, TX, 1973.
17. Hyde, D.W., "CONWEP: Conventional Weapons Effects Program," Waterways Experiment Station, Vicksburg, MS, 1991.
18. Chapman, T.C., Rose, T.A. and Smith, P.D., "Blast Wave Simulation Using AUTODYN2D: A Parametric Study," Int. J. Impact Engng., Vol. 16, pp. 777-787, 1995.
19. Drotleff, J.E., Vincent, C.T., Mullin, S.A., Walker, J.D. and Morris, B.L., "Research in Close-In Blast Loading from High Explosives," FMC Report, ARL-CR-308, September, 1996.
20. "LS-DYNA Release Notes, 940," Livermore Software Tech. Corp., 1997.
21. Souli, M. personal communication, 1997.
22. Condon, J.A., Gniazdowski, N. and Gregory, F.H., "The Design, Testing, and Analysis of a Proposed Composite Hull Technology Mine-Blast-Resistant Vehicle Floor Panel," ARL Final report ARL-TR-796, U.S. Army Research Laboratory, Aberdeen Proving Ground, MD, July, 1995.
23. Caiazzo, et al, "Development of Design Software and Material Failure Models for Fiber Reinforced Plastic Pressure Hulls", MSC Final Report TFR 3401/1437, Naval Surface Warfare Center, Carderock Division, Bethesda, MD, Contract No. N00167-93-C-0022, January 1994.
24. ABAQUS Finite Element Analysis Software, available from Hibbitt, Karlson and Sorensen, Inc., Providence, RI.

## GLOSSARY OF TERMS

3D Brick Elements	A type of finite element used to describe a 3D volume of material. These elements are used for modeling structures where an accurate three dimensional assessment of the stress state is required.
3D Failure Model	A material model used to determine onset of failure under a 3D stress condition developed from a 3D brick or thick shell model.
Anisotropic Material	A material where the subject properties are NOT independent of the direction of measurement.
AUGUST	A computational fluid mechanics code developed by Science Applications International Corp. (SAIC) for predicting shock wave and blast pressure distributions produced by an explosive detonation.
Composite Material	A artificial material composed of at least two phases, or constituents: - usually a fibrous reinforcement phase, and a cementitious matrix phase. A composite material may be isotropic, transversely isotropic, orthotropic, or anisotropic depending on the properties and distribution of the reinforcement and matrix.
Constitutive	Pertaining to the properties of the composite constituents: - fiber and matrix
Continuum	The assumption of material continuity.
CONWEP	A computational method for predicting blast pressures produced by detonation of an explosive charge, see Ref. 14.
Coulomb-Mohr	A recently postulated composite failure criterion based on Coulomb friction damage. See Ref. 8.
CTH	A commercial hydrodynamic analysis code.
Damage Function	An arbitrary function which relates the state of damage in a composite ply to the strength of the ply under that damage mechanism.
Delamination	A common failure mechanism in composite laminates whereby a crack develops parallel to the plane of the individual plies within the laminate. This crack can cause partial or complete separation of the laminate.
Deviatoric Strain/Stress	The non-pressure part (plasticity) of the strain/stress component.
DYNA3D	A finite element analysis code developed at Lawrence Livermore National Lab for prediction deformation and failure under dynamic loading situations. See also dynamic analysis code
Dynamic Event	An event whereby properties, shape, loads, etc. may vary as a function of time
Dynamic Analysis Code	An analysis code where the modeling formulation is compatible with large deformation and high strain rate events

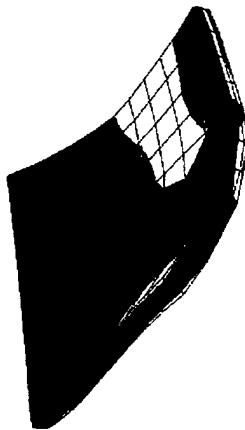
Equation of State	The relation between volume, pressure, and absolute temperature for a given mass of material.
Failure Criterion	A criterion for determining failure whereby the value of a given measure (stress, strain, energy), or combination of measures, is compared to a predetermined "failure" value for that measure of measures.
Fiber Breakage	A common failure mechanism in fibrous composites associated with the tensile, or compressive failure of the reinforcement fibers. This is a high stress failure mechanism associated with final failure of the laminate
Fiber Failure	See Fiber Breakage
Fiber/Matrix Cracking	A common failure mechanism in fibrous composites associated with separation of the fiber and matrix parallel to the fiber orientation under transverse load conditions. This is low stress ply failure mechanism which is not usually associated with final failure except in certain highly oriented laminates loaded in the transverse direction.
Heterogeneous Material	A material composed from at least two other constituent materials. Composites are heterogeneous. Heterogeneous materials may be isotropic, or anisotropic, etc.
Homogeneous	A material composed of a single constituent. Homogeneous materials may be isotropic, or anisotropic, etc.
Isotropic	A material where the subject properties are independent of the direction of measurement. An isotropic material may be heterogeneous, or homogeneous.
Lagrangian Finite Element Code	A finite element code based on a Lagrangian description - a description of elements based on the undeformed state which may subsequently deform and flow, but across whose boundaries material may not flow.
Laminate, Lamination, Laminae	An stack of multiple individual plies (laminae) arranged to suit the requirements of a given application. The creation of a laminate
LS-DYNA3D	The PC-version of DYNA3D marketed by KBS2 Inc.
Material Model	A mathematical model which describes one, or more aspects of the behavior of the material of interest: - deformation, failure, etc.
Matrix Shear	A failure mode in composite materials whereby separation takes place by shear failure of the matrix phase.
Mesh	The result of the discretization of the structural geometry into an arrangement of finite elements. A coarse mesh is composed of few, large elements. A fine mesh is composed of many,, small elements. The mesh size determines both the accuracy of the results (fine - more accurate), and the computational efficiency of the model (coarse - runs faster).



Micromechanics	A material modeling approach used in composites whereby the properties of the material are derived from an examination of the properties and arrangement of the constituent materials.
Mixture Theory	A theory which states that the properties of a mixture are dependent on the properties of the mixture constituents and their relative proportions within the mixture.
Orthotropic	A material which exhibits three perpendicular planes of symmetry.
Plasticity Theory	A theory used to describe the behavior of materials in the non-elastic regime.
Ply	The basic building block of a laminate. A single layer of unidirectional tape or woven cloth.
Ply Separation	The separation of plies parallel to their plane. See also delamination.
Progressive Failure	A failure process characterized by a succession of individual failure events of increasing severity.
Quasi-Static Event	An event whereby changes in shape, properties, load, etc., are not considered as a function of time.
Sandwich Panel	A composite construction designed for high bending rigidity, and low weight, usually characterized by two composite laminates (face sheets) separated by a low density foam, balsa, or honeycomb core.
Sub-Cycling Numerical Scheme	A numerical scheme whereby detailed calculation of local effects are conducted outside the main solution routine.
Thick Shell Elements	A type of finite element used for modeling structures where thickness is small compared to the other dimensions. However, the element formulation allows an approximation of the element stress state in the thickness direction.
Thin Shell Elements	A type of finite element used for modeling structures where thickness is small compared the other dimensions. The stress state in the thickness direction is not formulated.
Transversely Isotropic	A material with isotropic symmetry in one plane. A unidirectional ply is transversely
Unidirectional	A composite material construction where all the fibers are oriented in a single direction.
User-Defined Module	A user-created module which may be introduced into a computational solution routine, or code, for determining effects or results of interest to the user. LS-DYNA3D allows the introduction of user-defined material models for dynamic analysis of structures composed of non-traditional materials.

SIMPLY SUPPORTED SANDWICH PLATE  
time = 1.47968E-03  
fringe = y-stress  
min = -2.408E+05 in element 01  
max = 2.408E+05 in element 01  
integration point = 1

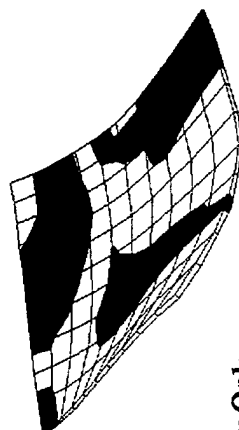
fringe levels  
1 -2.408E+05  
2 -1.605E+05  
3 -8.02E+04  
4 0.00E+00  
5 8.02E+04  
6 1.605E+05  
7 2.408E+05



$\bar{z}$   
 $\bar{y}$  Full Panel

SIMPLY SUPPORTED SANDWICH PLATE  
time = 1.47968E-03  
fringe = y-stress  
min = -2.408E+05 in element 01  
max = 2.408E+05 in element 01  
integration point = 1

fringe levels  
1 -2.408E+05  
2 -1.605E+05  
3 -8.02E+04  
4 0.00E+00  
5 8.02E+04  
6 1.605E+05  
7 2.408E+05

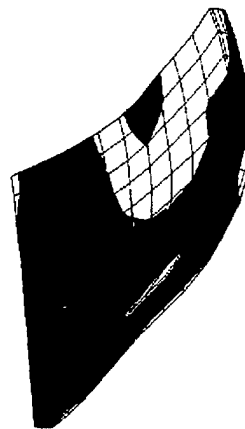


$\bar{z}$   
 $\bar{y}$  Critical Ply Only

(a) Axial Stress Contours at 1.48 milli-sec, No Element Failure

SIMPLY SUPPORTED SANDWICH PLATE  
time = 1.58981E-03  
fringe = y-stress  
min = -2.395E+05 in element 01  
max = 2.395E+05 in element 01  
integration point = 1

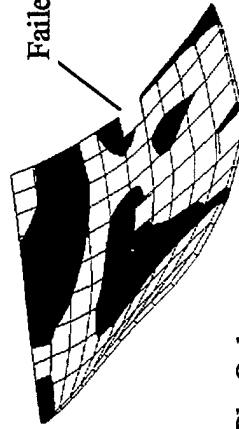
fringe levels  
1 -2.395E+05  
2 -1.593E+05  
3 -7.96E+04  
4 0.00E+00  
5 7.96E+04  
6 1.593E+05  
7 2.395E+05



$\bar{z}$   
 $\bar{y}$  Full Panel

SIMPLY SUPPORTED SANDWICH PLATE  
time = 1.58981E-03  
fringe = y-stress  
min = -2.395E+05 in element 01  
max = 2.395E+05 in element 01  
integration point = 1

fringe levels  
1 -2.395E+05  
2 -1.593E+05  
3 -7.96E+04  
4 0.00E+00  
5 7.96E+04  
6 1.593E+05  
7 2.395E+05



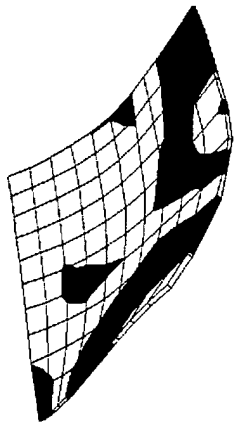
$\bar{z}$   
 $\bar{y}$  Critical Ply Only

(b) Axial Stress Contours at 1.59 milli-sec, After Element Failure

Figure 1. Demonstration of Progressive Failure Capability for Composite Sandwich Panel.

SIMPLY SUPPORTED SANDWICH PLATE  
 time = 1.47956E-03  
 fringes at z=stress  
 min=-0.490E+03 in element 91  
 max=1.599E+04 in element 92  
 integration point = 1

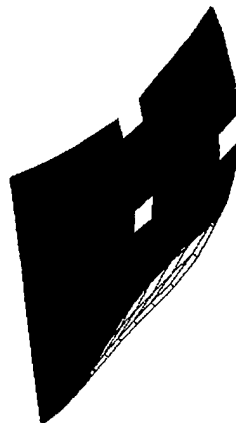
fringe levels  
 1 0.000E+00  
 2 0.375E+03  
 3 0.750E+03  
 4 1.125E+03  
 5 1.500E+03  
 6 1.875E+03  
 7 2.250E+03  
 8 2.625E+03  
 9 3.000E+03



$\begin{matrix} z \\ \downarrow \\ x-y \end{matrix}$  Axial Stress in Bottom Most 0-Layer

SIMPLY SUPPORTED SANDWICH PLATE  
 time = 1.58901E-03  
 fringes at z=stress  
 min=-1.429E+03 in element 91  
 max=1.599E+04 in element 92  
 integration point = 1

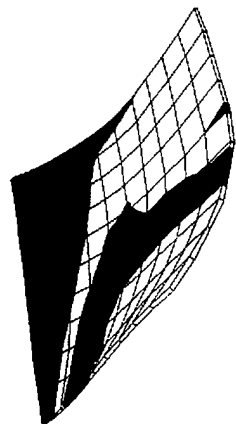
fringe levels  
 1 0.000E+00  
 2 0.375E+03  
 3 0.750E+03  
 4 1.125E+03  
 5 1.500E+03  
 6 1.875E+03  
 7 2.250E+03  
 8 2.625E+03  
 9 3.000E+03



$\begin{matrix} z \\ \downarrow \\ x-y \end{matrix}$  Axial Stress in Bottom Most 0-Layer

SIMPLY SUPPORTED SANDWICH PLATE  
 time = 1.47956E-03  
 fringes at z=stress  
 min=-0.490E+03 in element 91  
 max=1.599E+04 in element 92  
 integration point = 1

fringe levels  
 1 0.000E+00  
 2 0.375E+03  
 3 0.750E+03  
 4 1.125E+03  
 5 1.500E+03  
 6 1.875E+03  
 7 2.250E+03  
 8 2.625E+03  
 9 3.000E+03

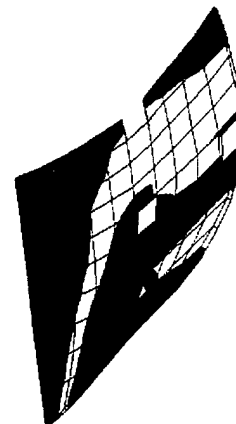


$\begin{matrix} z \\ \downarrow \\ x-y \end{matrix}$  Through Thickness Shear in Bottom Most 90-Layer

(a) Stress Contours at 1.48 milli-sec,  
 No Element Failure

SIMPLY SUPPORTED SANDWICH PLATE  
 time = 1.58901E-03  
 fringes at z=stress  
 min=-1.429E+03 in element 91  
 max=1.599E+04 in element 92  
 integration point = 1

fringe levels  
 1 0.000E+00  
 2 0.375E+03  
 3 0.750E+03  
 4 1.125E+03  
 5 1.500E+03  
 6 1.875E+03  
 7 2.250E+03  
 8 2.625E+03  
 9 3.000E+03

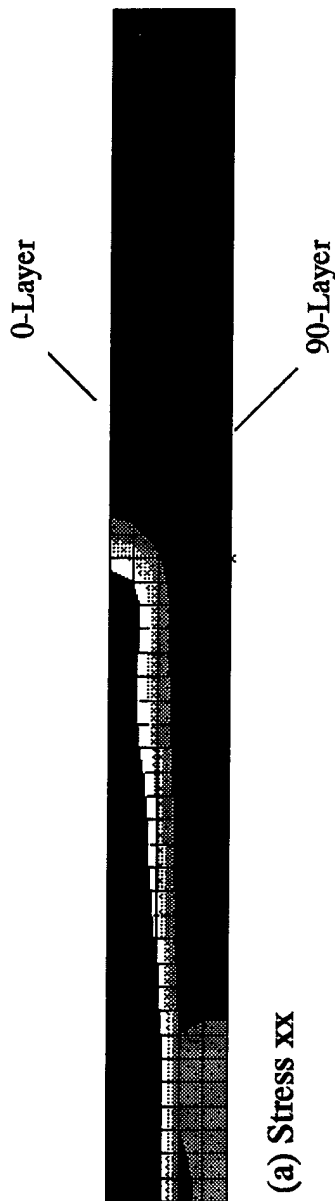


$\begin{matrix} z \\ \downarrow \\ x-y \end{matrix}$  Through Thickness Shear in Bottom Most 90-Layer

(b) Stress Contours at 1.59 milli-sec,  
 After Element Failure

Figure 2. Demonstration of Ply-By-Ply 3D Stress and Failure Analysis Capabilities.

LS-DYNA3D user input  
 STEP 7 TIME = 1.3763255E-005  
 SIGZZ (MID)



1.5430E+001  
 -9.2800E+003  
 -1.8572E+004  
 -2.7888E+004  
 -3.7144E+004  
 -4.6400E+004  
 -5.5711E+004  
 -6.5035E+004  
 -7.4289E+004  
 -8.3575E+004  
 -9.2861E+004  
 -9.2861E+004

LS-DYNA3D user input  
 STEP 7 TIME = 1.3763255E-005  
 SIGYZ (MID)



6.5387E+001  
 -6.5789E+002  
 -1.3006E+003  
 -2.1038E+003  
 -2.8269E+003  
 -3.5500E+003  
 -4.2731E+003  
 -4.9962E+003  
 -5.7192E+003  
 -6.4423E+003  
 -7.1654E+003  
 -7.1654E+003

Figure 3. Demonstration of Potential Shock Wave Delamination Failure Mode: High Interply Shear Stress Resulted due to In-Plane Shock Waves in [0/90] Laminate.

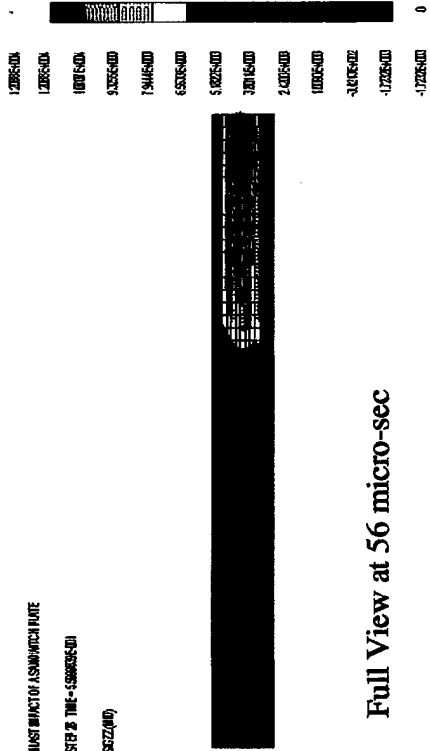
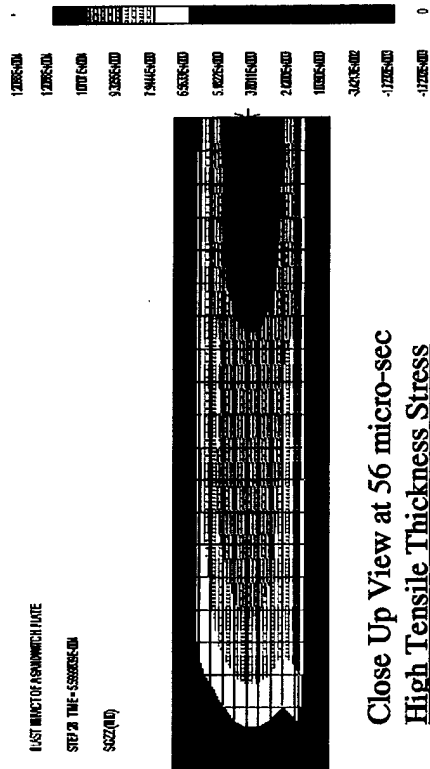
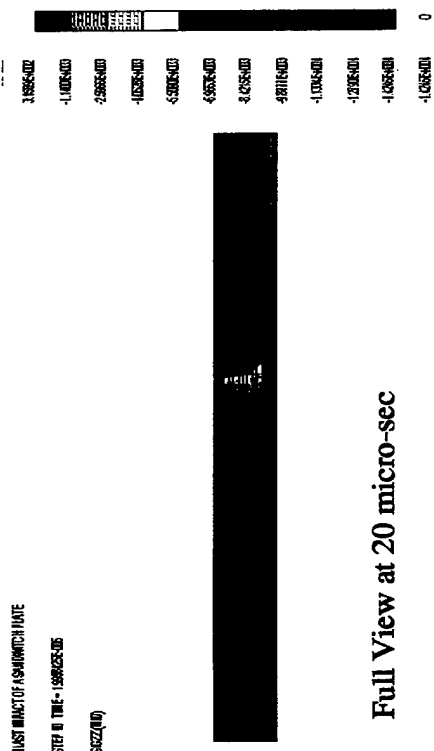
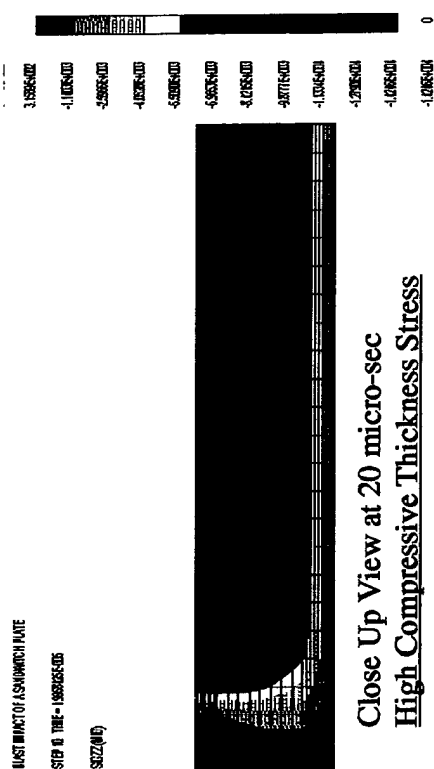


Figure 4. Demonstration of Potential Through the Thickness Failure Modes of Matrix Compression and Ply Separation Induced by Through the Thickness Blast Shock Waves in Composite Sandwich Panel.

STEP 50 TIME = 2.453595E-03

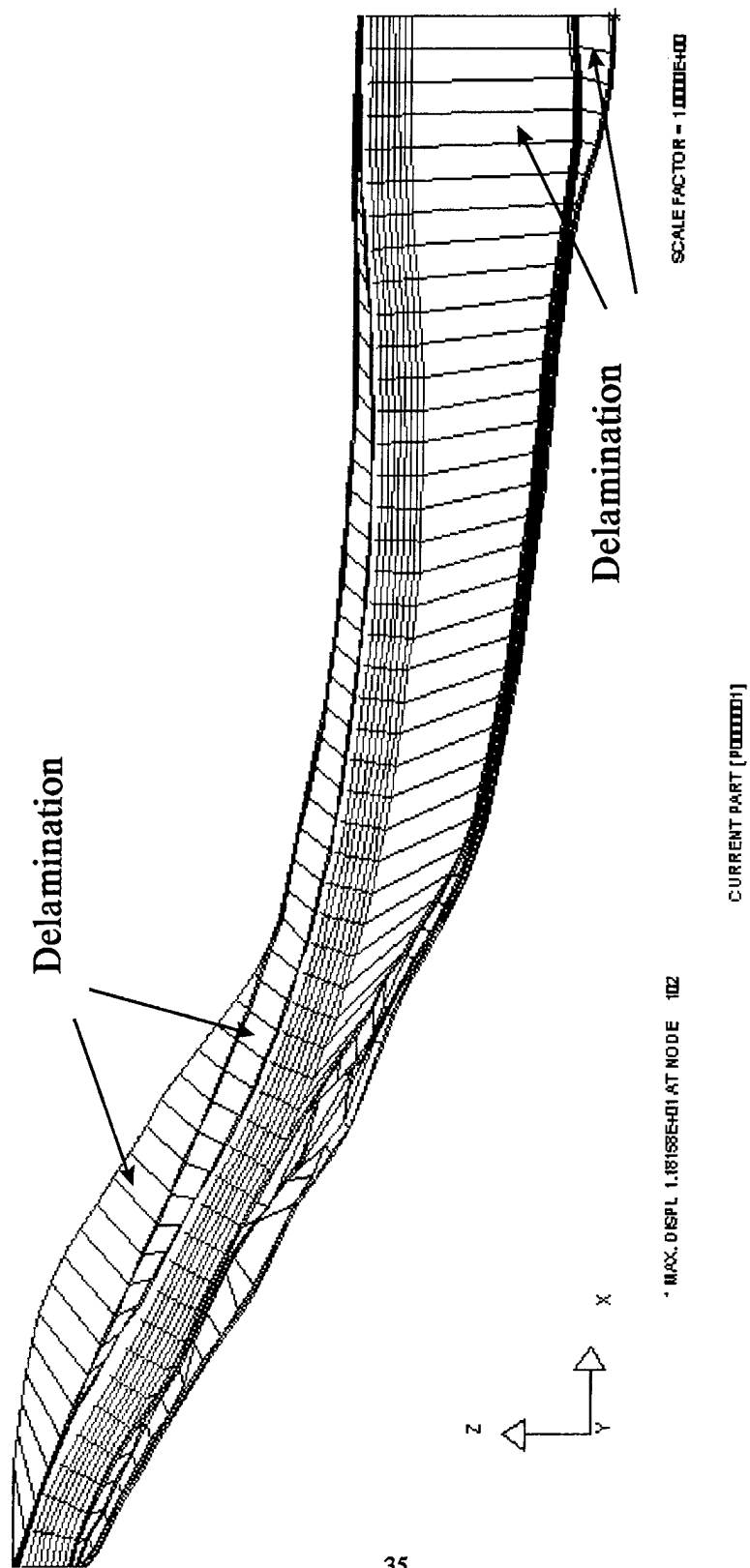


Figure 5. MSC Material Models Integrated into LS-DYNA3D Allow Simulation of Progressive Delamination Failure in Composite Sandwich Panel under Mine Blast Condition.

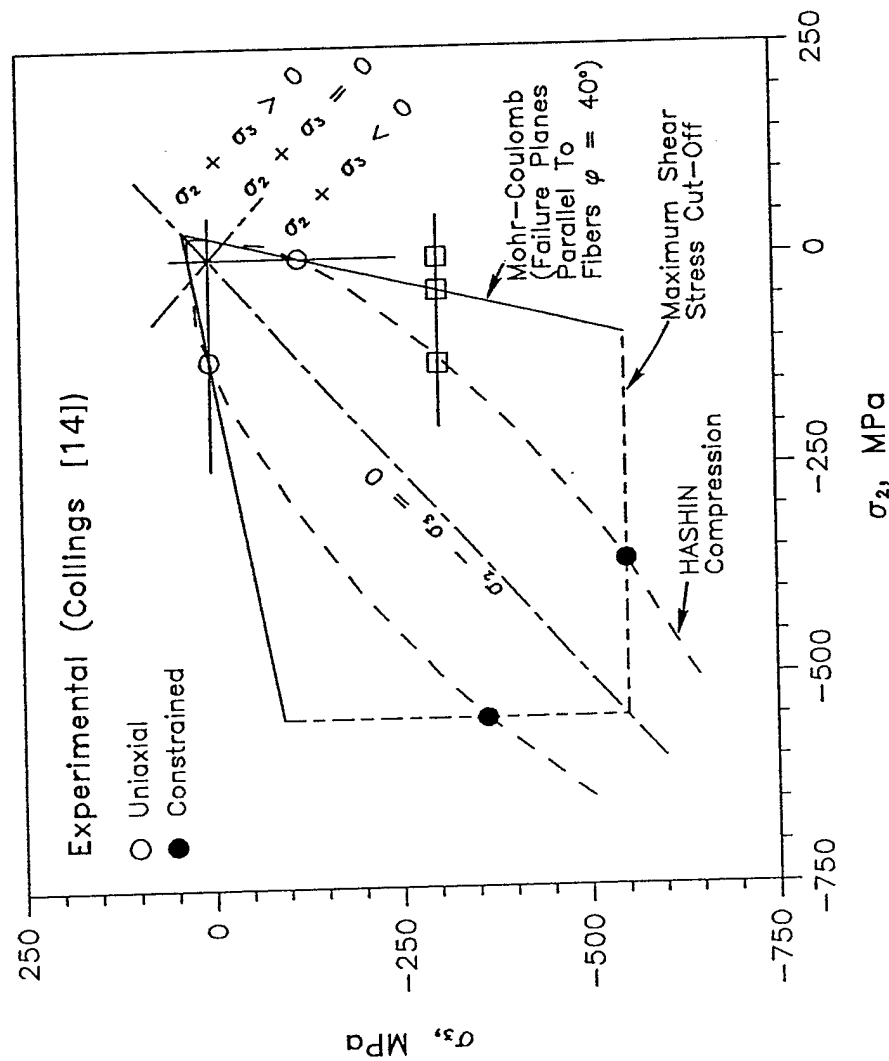


Figure 6. Plane Stress Failure Surfaces Of Mohr-Coulomb Model And Hashin Compression Model For A Composite Tested By Collings [14].

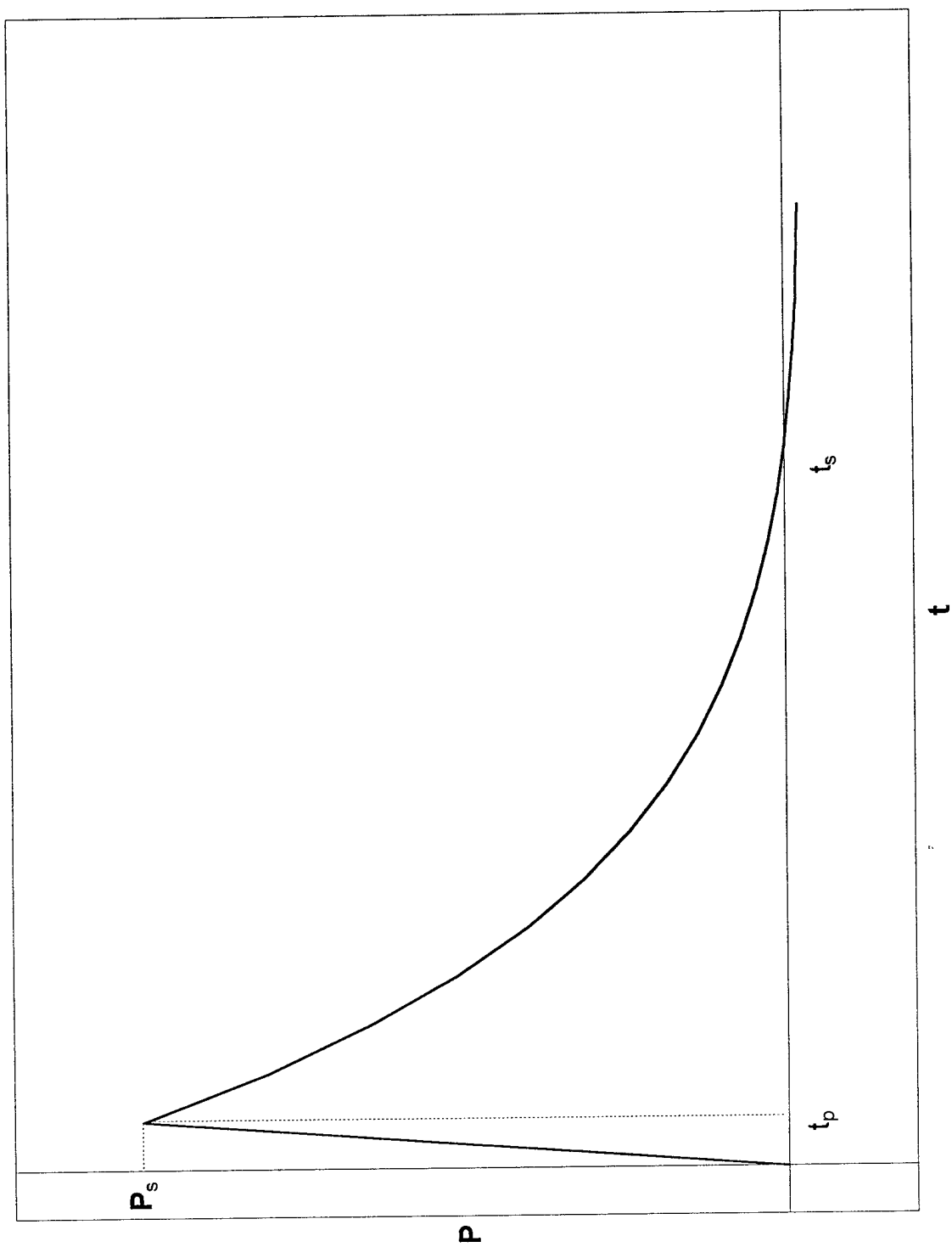


Figure 7. Blast Wave Load-Time Curve Representations.



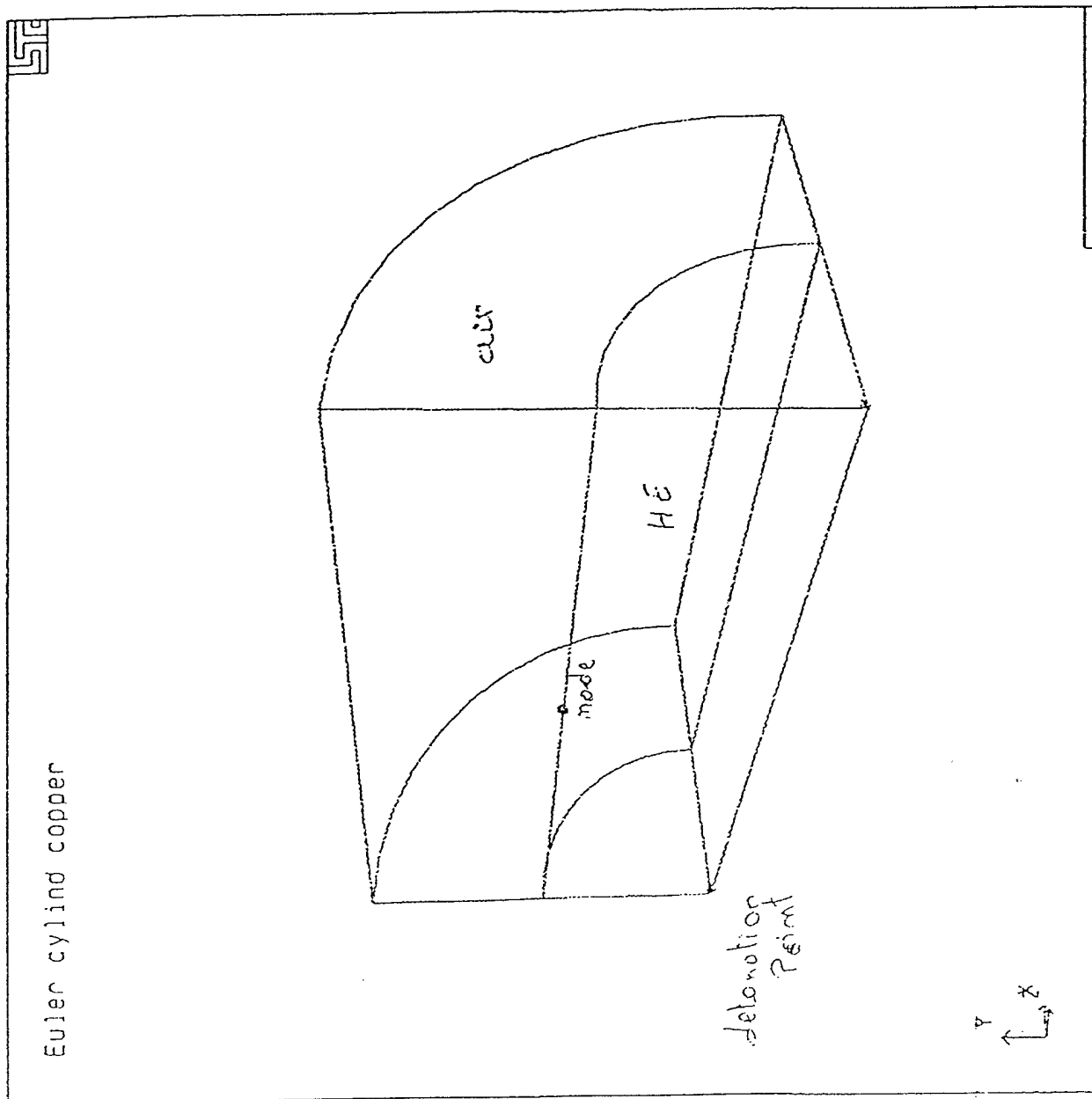


Figure 8a. A 3D Eulerian Grid for a Tube with High Explosive Mesh Inside and Air Mesh Outside

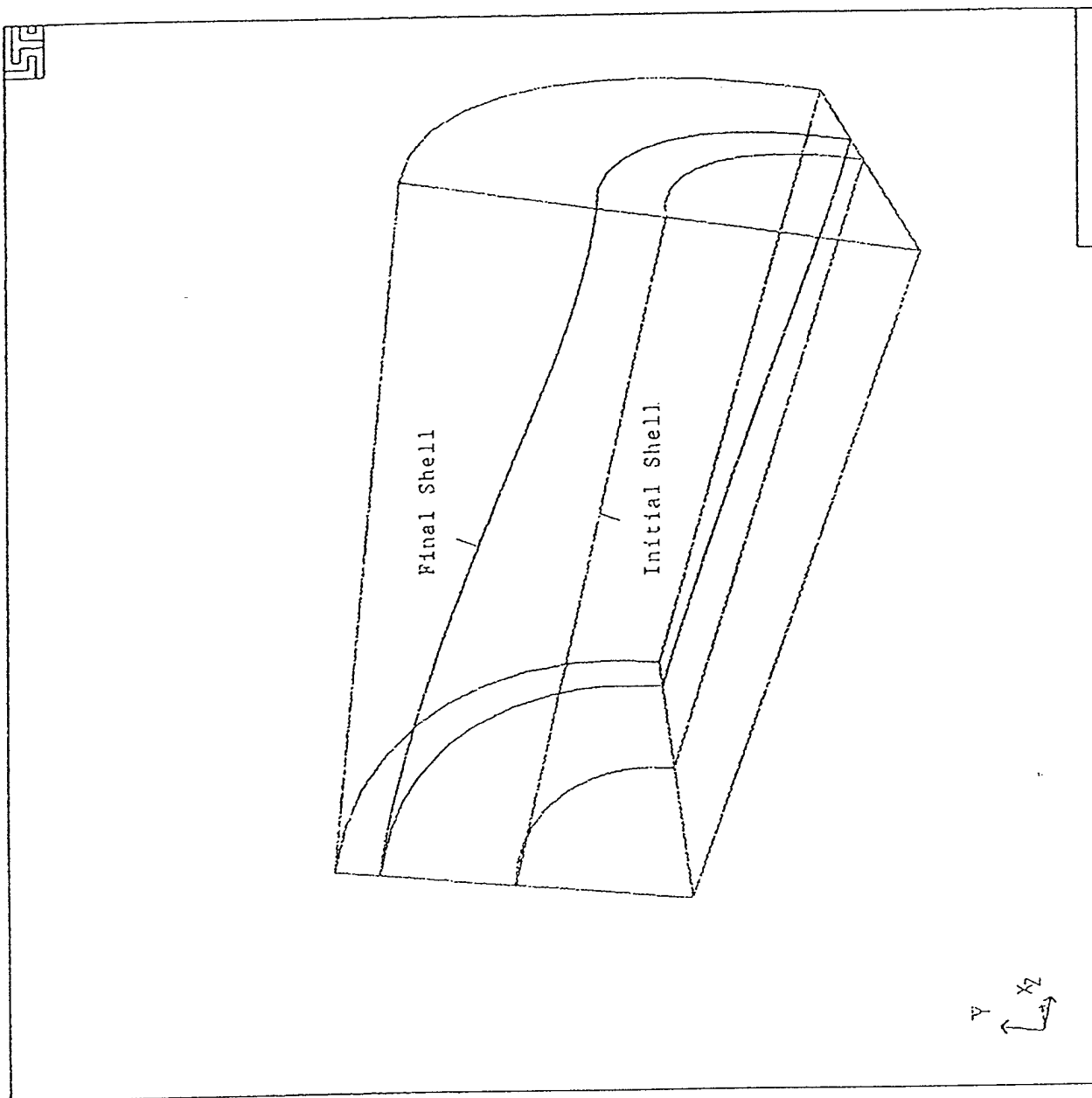


Figure 8b. Initial and Final Geometry of the Cylinder after Deformation

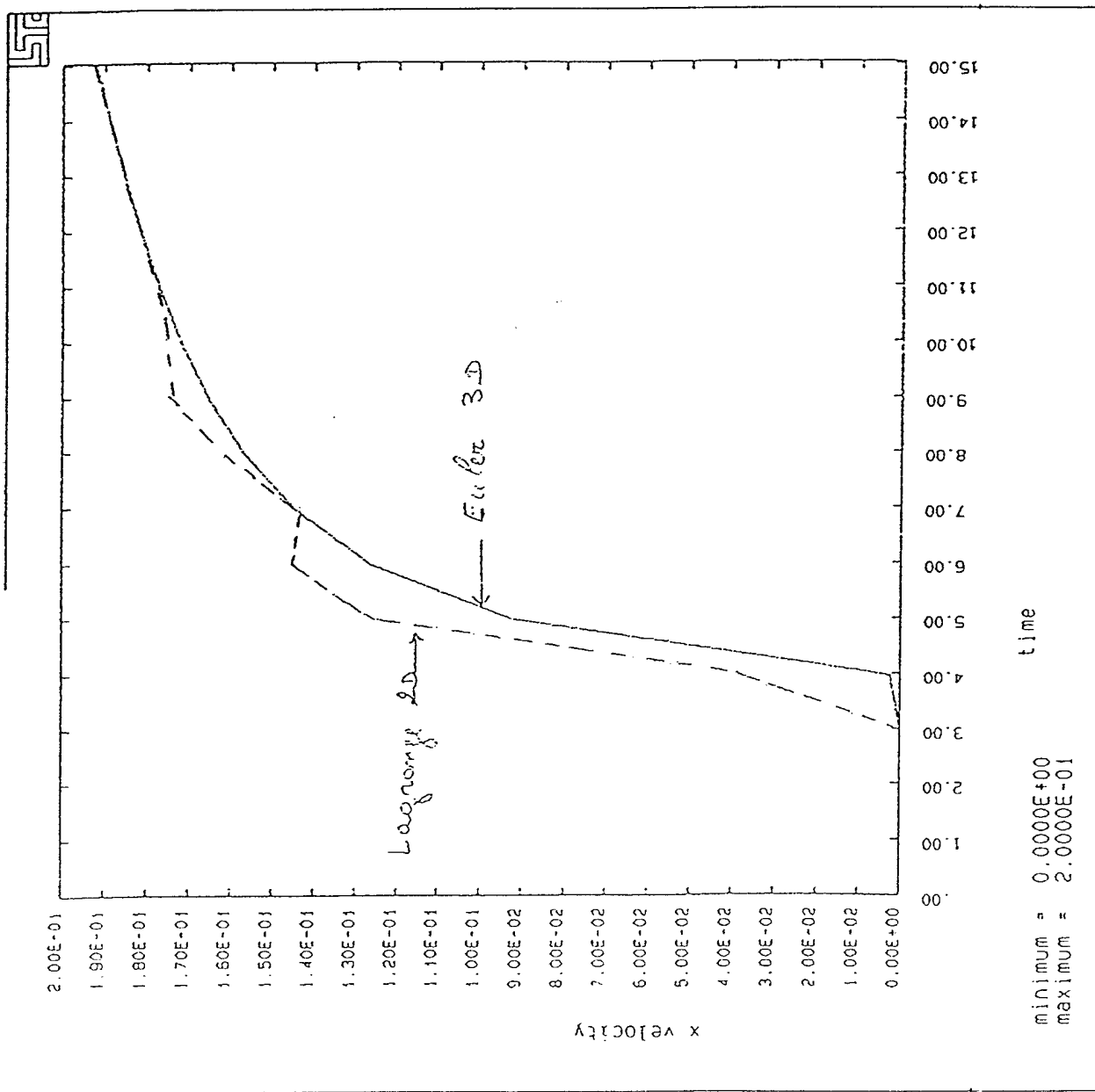


Figure 9a. Velocity History at a Note on the Tube

Euler 3D  
 Lagrange 2D

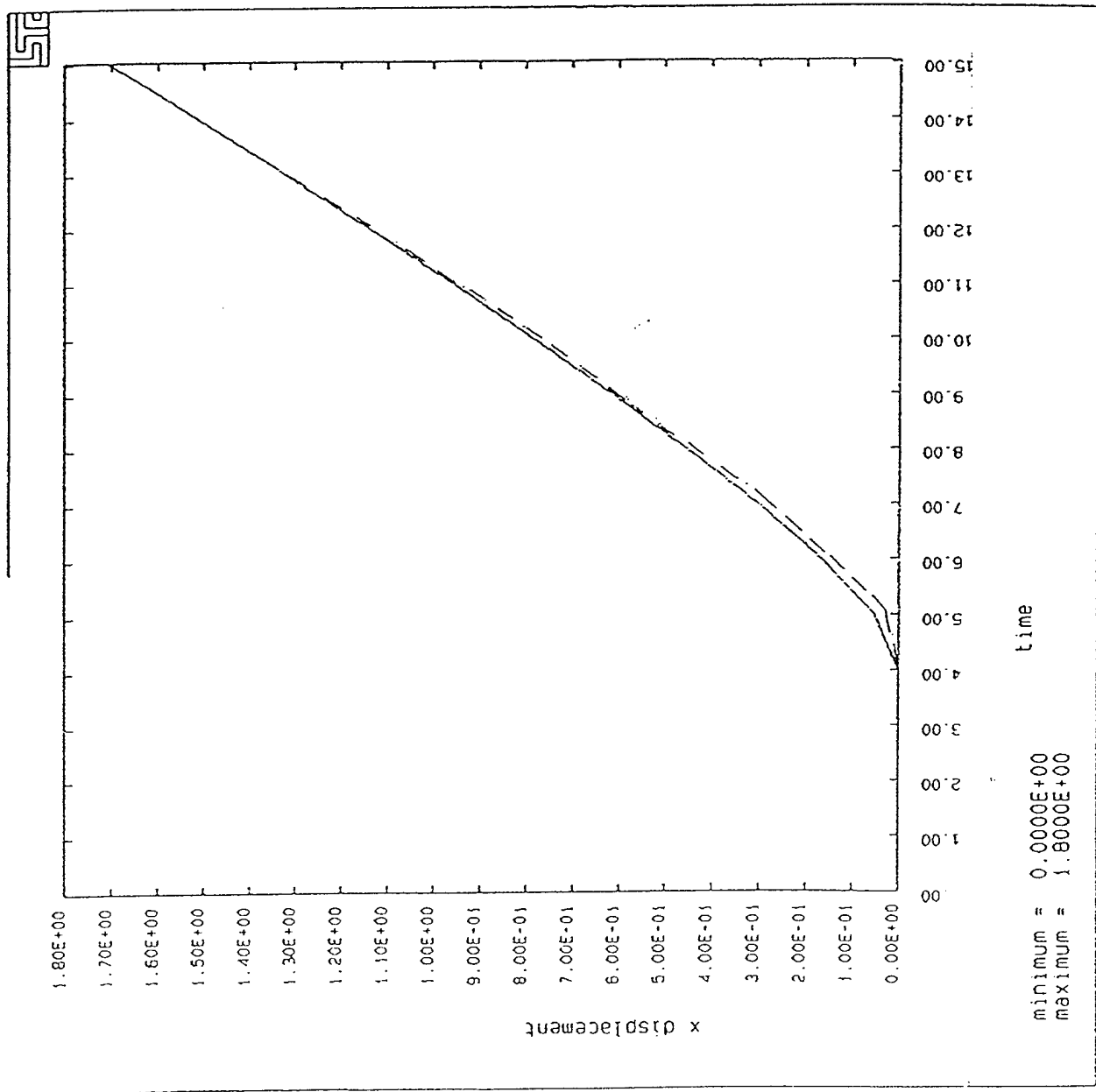
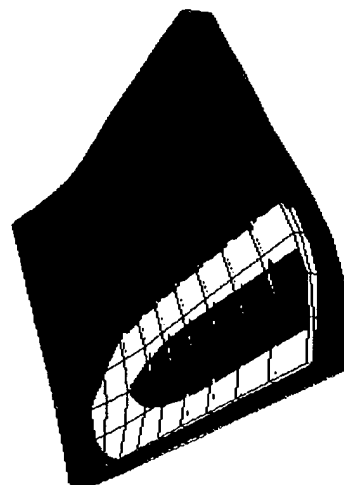
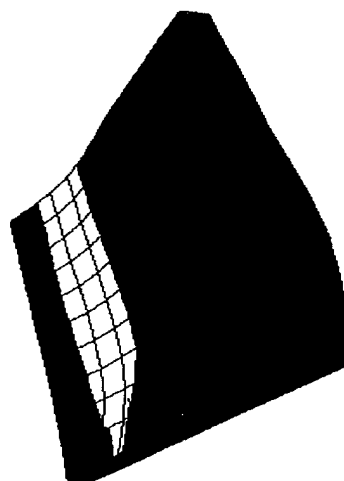


Figure 9b. Displacement History at a Node on the Tube



z

z

(a) Stress  $\sigma$

(b) Stress  $\tau$

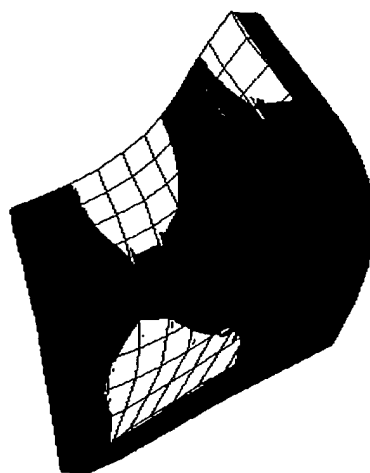
Figure 10. Stress Distribution in Sandwich Plate, 0.5 milli-sec.

11

# SIMPLY SUPPORTED SANDWICH PLATE

time = 1.00893E-03  
 fringes of  $\sigma$ -stress  
 min = -7.382E+04 in element 340  
 max = 8.321E+04 in element 55  
 integration point # 2

fringe levels  
 -7.382E+04  
 -4.765E+04  
 -2.148E+04  
 4.593E+03  
 3.896E+04  
 5.704E+04  
 8.321E+04



z  
y  
x

FIGURE 11.11 (a) STRESS XX

(a) Stress xx

# SIMPLY SUPPORTED SANDWICH PLATE

time = 1.00893E-03  
 fringes of  $\sigma$ -stress  
 min = -9.614E+04 in element 53  
 max = 7.958E+04 in element 393  
 integration point # 2

fringe levels  
 -9.614E+04  
 -6.685E+04  
 -3.756E+04  
 -8.277E+03  
 2.101E+04  
 5.030E+04  
 7.958E+04

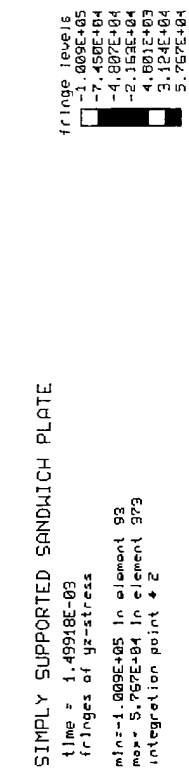


z  
y  
x

FIGURE 11.11 (b) STRESS YZ

(b) Stress yz

Figure 11. Stress Distribution in Sandwich Plate, 1.0 milli-sec.



(a) Stress  $\sigma_x$



(b) Stress  $\sigma_y$

Figure 12. Stress Distribution in Sandwich Plate, 1.5 milli-sec.

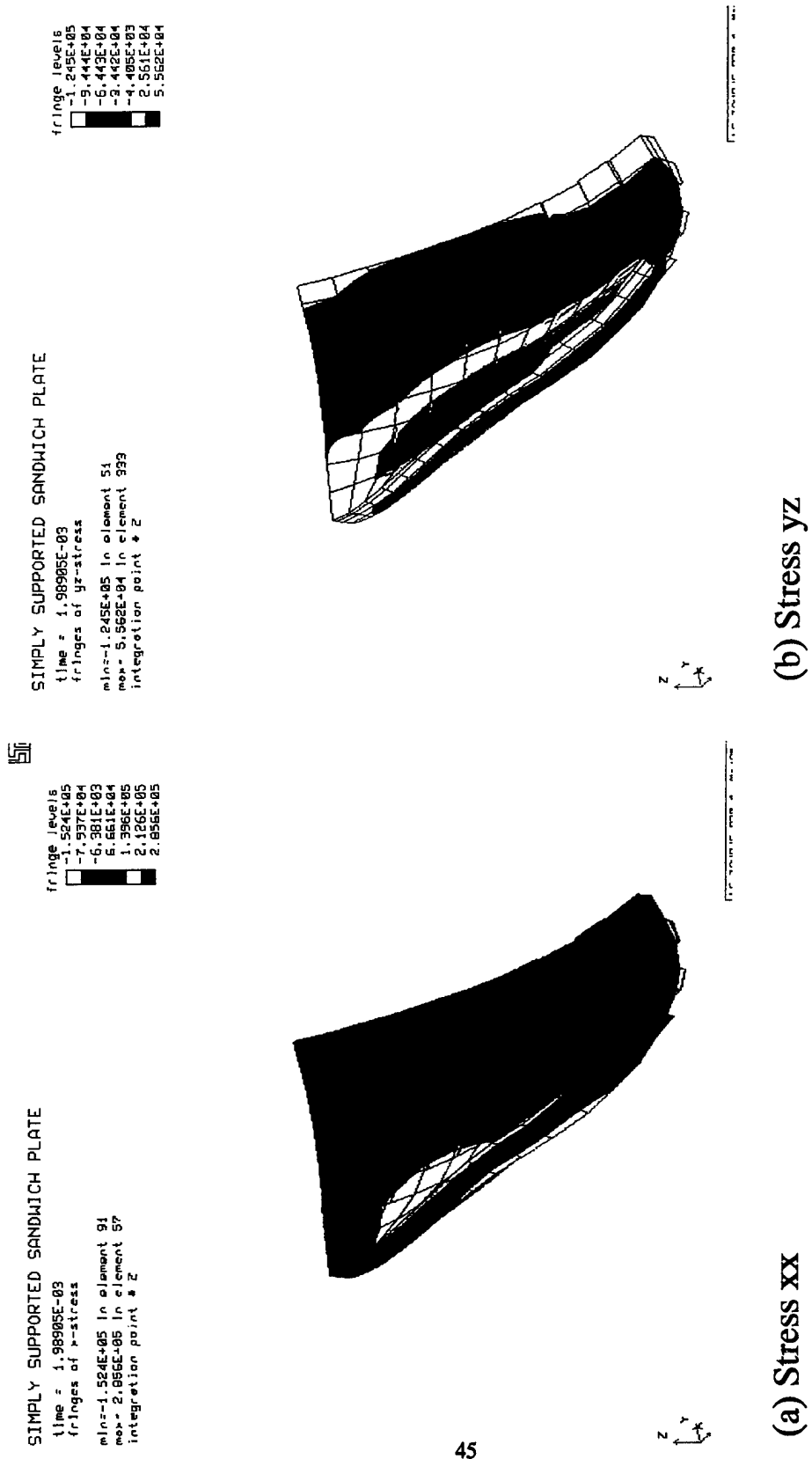
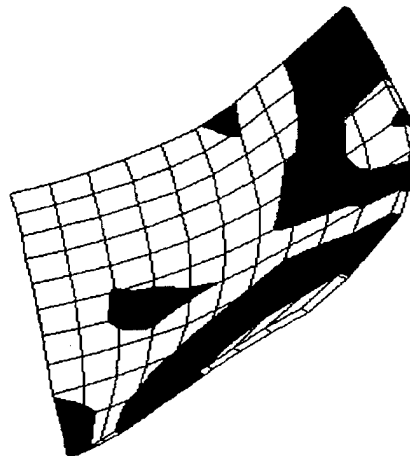


Figure 13. Stress Distribution in Sandwich Plate, 2.0 milli-sec.

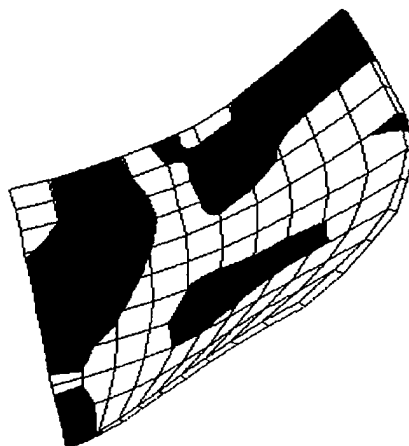


SIMPLY SUPPORTED SANDWICH PLATE  
 time = 1.46922E-03  
 fringes of  $\sigma$ -stress  
 min=-4.844E+05  
 max= 2.491E+05  
 integration point # 1

SIMPLY SUPPORTED SANDWICH PLATE  
 time = 1.46922E-03  
 fringes of  $\sigma$ -stress  
 min=-4.844E+05  
 max= 2.491E+05  
 integration point # 1



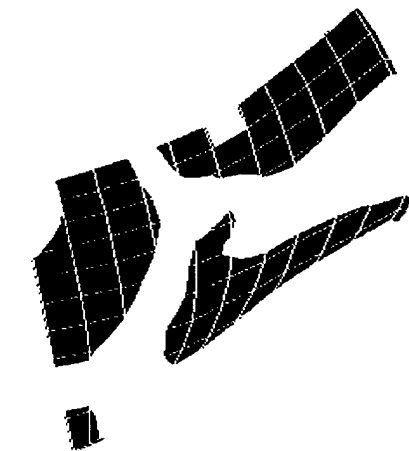
(b) Outmost 0 layer



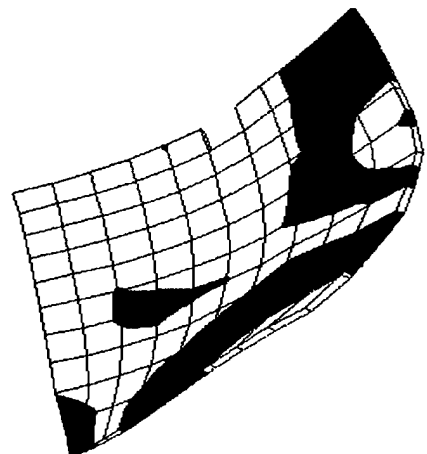
(a) Outmost 90 layer

Figure 14. Layer Axial Stresses in Bottom Face Sheet, 1.47 milli-sec.

SIMPLY SUPPORTED SANDWICH PLATE  
 time = 1.48997E-03  
 fringes of  $\nu$ -stress  
 min = -4.101E+05 in element 91  
 max = 2.500E+05 in element 76  
 integration point # 1



(a) Outmost 90 layer

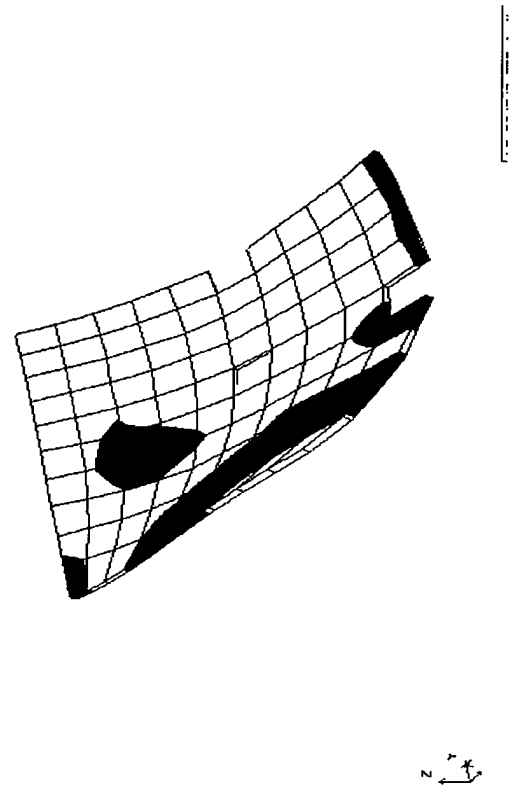


(b) Outmost 0 layer

Figure 15. Layer Axial Stresses in Bottom Face Sheet, 1.49 milli-sec.



(a) Outmost 90 layer



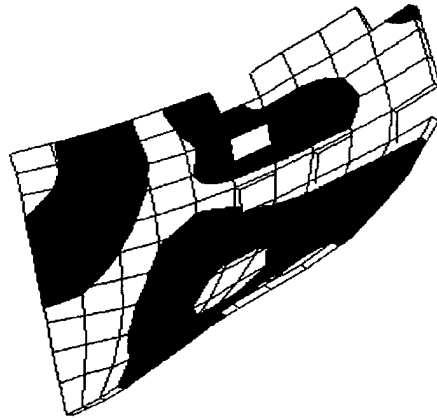
(b) Outmost 0 layer

Figure 16. Layer Axial Stresses in Bottom Face Sheet, 1.59 milli-sec.

# SIMPLY SUPPORTED SANDWICH PLATE

time = 1.68922E-03  
fringes of y-stress  
min=-4.706E+05 in element 10  
max= 2.017E+05 in element 78  
integration point # 2

fringe levels  
-4.706E+05  
-3.585E+05  
-2.465E+05  
-1.344E+05  
-2.237E+04  
8.968E+04  
2.017E+05



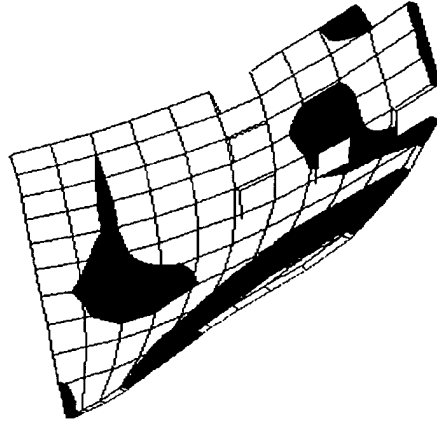
1E+05 MPa 4 MAX

(a) Outmost 90 layer

# SIMPLY SUPPORTED SANDWICH PLATE

time = 1.68922E-03  
fringes of x-stress  
min=-4.476E+05 in element 91  
max= 2.316E+05 in element 90  
integration point # 1

fringe levels  
-4.476E+05  
-3.344E+05  
-2.212E+05  
-1.080E+05  
5.133E+03  
1.104E+05  
2.316E+05

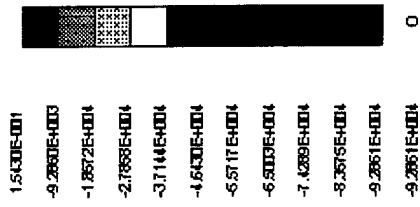


1E+05 MPa 4 MAX

(b) Outmost 0 layer

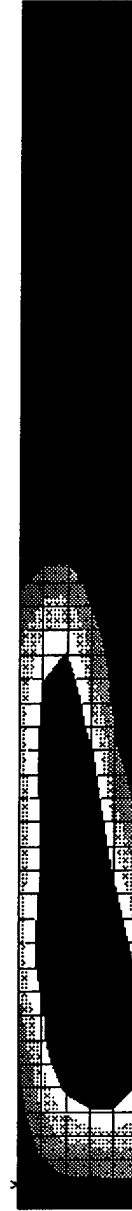
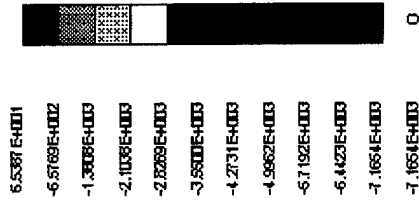
Figure 17. Layer Axial Stresses in Bottom Face Sheet, 1.69 milli-sec.

LS-DYNA3D user input  
 STEP 7 TIME = 1.3763258E-05  
 SIGZZ (MID)



(a) Stress xx

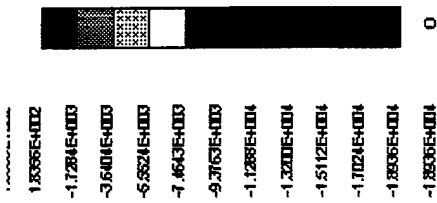
LS-DYNA3D user input  
 STEP 7 TIME = 1.3763258E-05  
 SIGYZ (MID)



(b) Stress xz

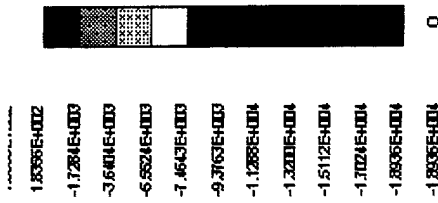
Figure 18. In-Plane Shock Waves in [0/90]<sub>n</sub>, 1.38 micro-sec.

BLAST IMPACT OF A SANDWICH PLATE  
 STEP 5 TIME = 9.5216630E-006  
 SIGZZ (MID)



(a) Stress zz, Full View

BLAST IMPACT OF A SANDWICH PLATE  
 STEP 5 TIME = 9.5216630E-006  
 SIGZZ (MID)



(b) Stress zz, Close Up

Figure 19. Through the Thickness Shock Waves in Sandwich Plate, 10 micro-sec.

BLAST IMPACT OF A SANDWITCH PLATE

STEP 10 TIME = 1.9851425E-005

SIGZZ(MID)

3.1539E+002  
-1.1403E+003  
-2.5965E+003  
-4.0528E+003  
-5.5000E+003  
-6.9633E+003  
-8.4215E+003  
-9.8777E+003  
-1.1334E+004  
-1.2790E+004  
-1.4246E+004  
-1.4246E+004



(a) Stress zz, Full View

BLAST IMPACT OF A SANDWITCH PLATE

STEP 10 TIME = 1.9851425E-005

SIGZZ(MID)

3.1539E+002  
-1.1403E+003  
-2.5965E+003  
-4.0528E+003  
-5.5000E+003  
-6.9633E+003  
-8.4215E+003  
-9.8777E+003  
-1.1334E+004  
-1.2790E+004  
-1.4246E+004  
-1.4246E+004



(b) Stress zz, Close Up

Figure 20. Through the Thickness Shock Waves in Sandwich Plate, 20 micro-sec.

BLAST IMPACT OF A SANDWICH PLATE

STEP 25 TIME = 4.999853E-005

SIGZZ(MID)



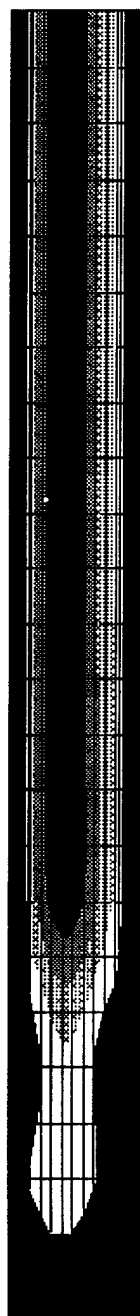
8.2117E+003  
6.9444E+003  
5.6705E+003  
4.4056E+003  
3.1423E+003  
1.8749E+003  
6.0755E+002  
-6.5978E+002  
-1.9271E+003  
-3.1945E+003  
-4.4618E+003  
-4.4618E+003

(a) Stress zz, Full View

BLAST IMPACT OF A SANDWICH PLATE

STEP 25 TIME = 4.999853E-005

SIGZZ(MID)



8.2117E+003  
6.9444E+003  
5.6705E+003  
4.4056E+003  
3.1423E+003  
1.8749E+003  
6.0755E+002  
-6.5978E+002  
-1.9271E+003  
-3.1945E+003  
-4.4618E+003  
-4.4618E+003

(b) Stress zz, Close Up

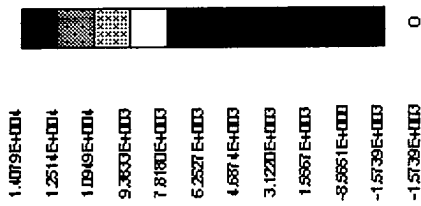
Figure 21. Through the Thickness Shock Waves in Sandwich Plate, 50 micro-sec.



BLAST IMPACT OF A SANDWICH PLATE

STEP 56 TIME = 1.119432E-004

SGZZ(MID)

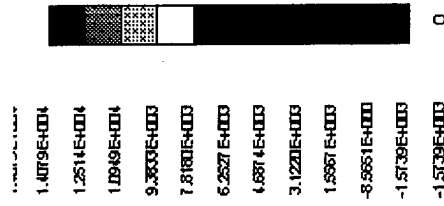


(a) Stress zz, Full View

BLAST IMPACT OF A SANDWICH PLATE

STEP 56 TIME = 1.119432E-004

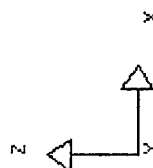
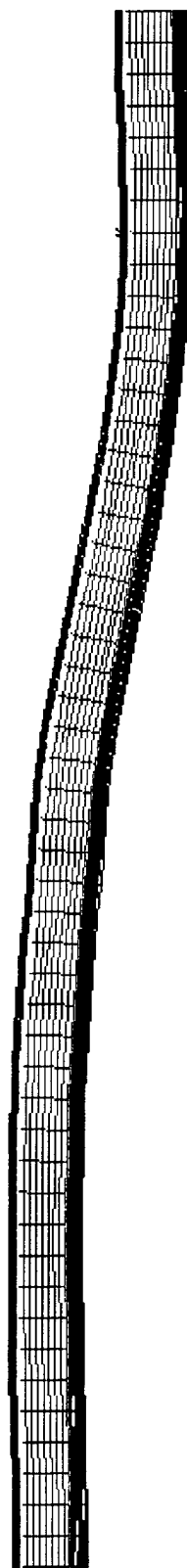
SGZZ(MID)



(b) Stress zz, Close Up

Figure 22. Through the Thickness Shock Waves in Sandwich Plate, 112 micro-sec.

STEP 10 TIME = 4.9986184E-004



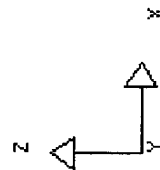
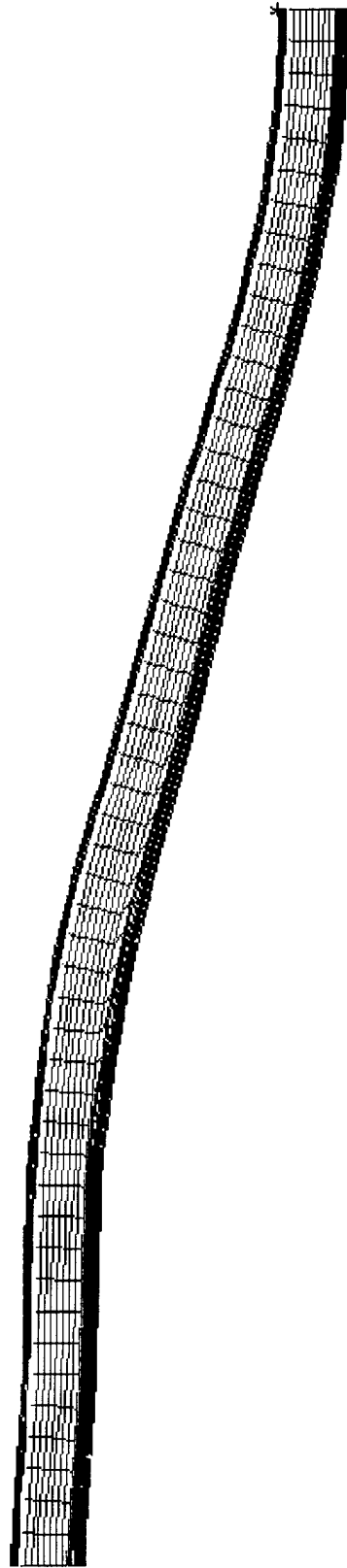
\* MAX. DISPL 2.35000E+001 AT NODE 2434

SCALE FACTOR = 1.000E+00

CURRENT PART (0000001)

Figure 23. Response of a Half of Sandwich Panel with S2/Epoxy Face Sheets Subjected to Blast Load - Demonstration of Delamination Progression at 0.5 msec.

STEP 20 TIME = 9.999539E-004



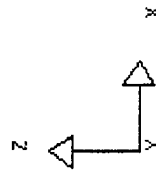
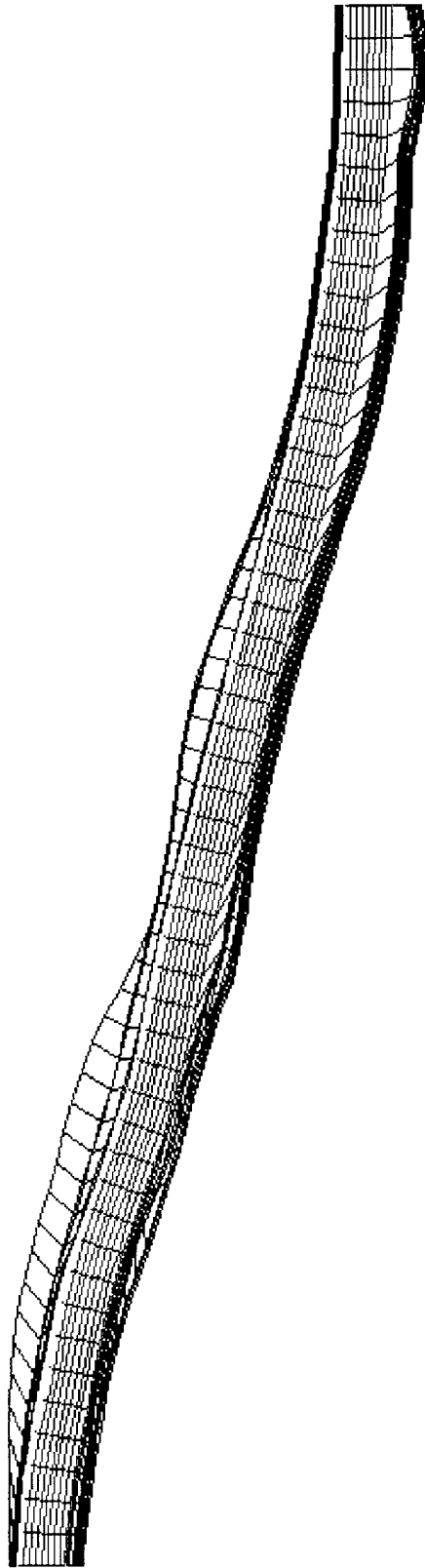
\* MAX. DISPL 5.91420E+001 AT NODE 2852

CURRENT PART (P000001)

SCALE FACTOR = 1.000E+00

Figure 24. Response of a Half of Sandwich Panel with S2/Epoxy Face Sheets Subjected to Blast Load - Demonstration of Delamination Progression at 1.0 msec.

STEP 30 TIME = 1.099905E-003



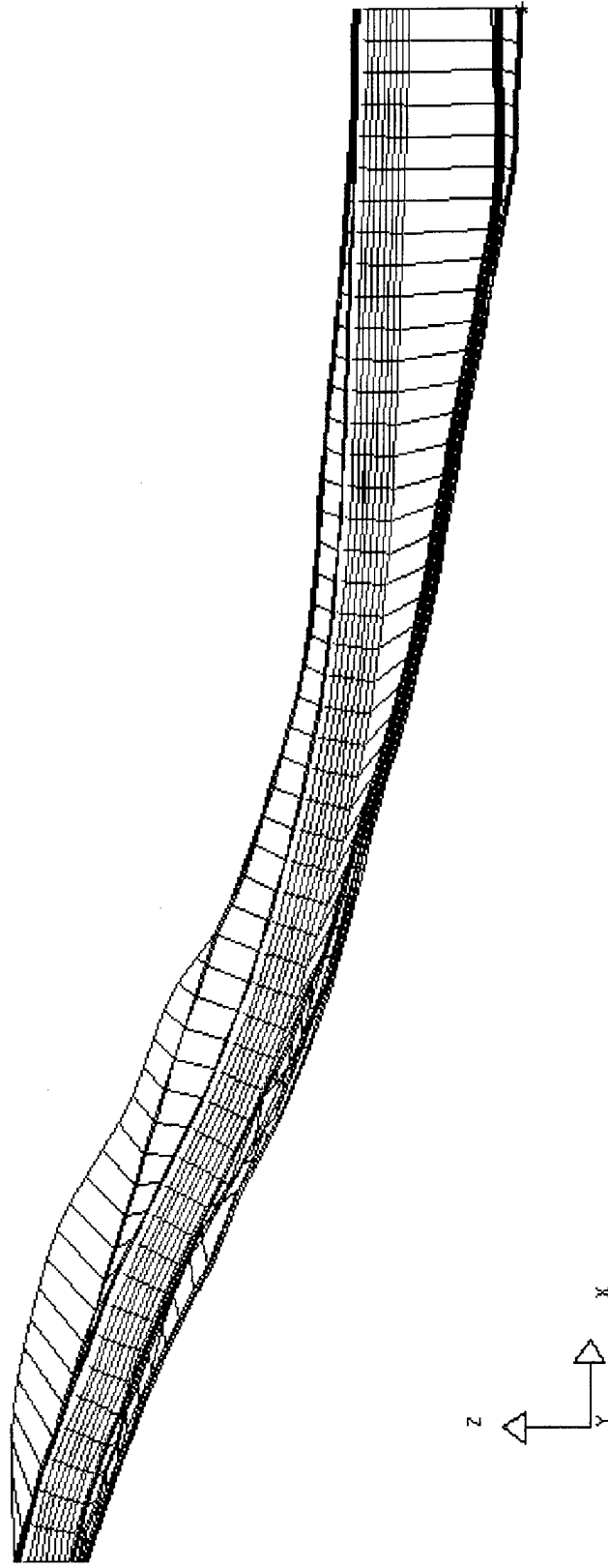
\* MAX. DISPL 7.791835E-001 AT NODE 603

CURRENT PART (P0000001)

SCALE FACTOR = 1.0000E+00

Figure 25. Response of a Half of Sandwich Panel with S2/Epoxy Face Sheets Subjected to Blast Load - Demonstration of Delamination Progression at 1.5 msec.

STEP 40 TIME = 1.999999E-003



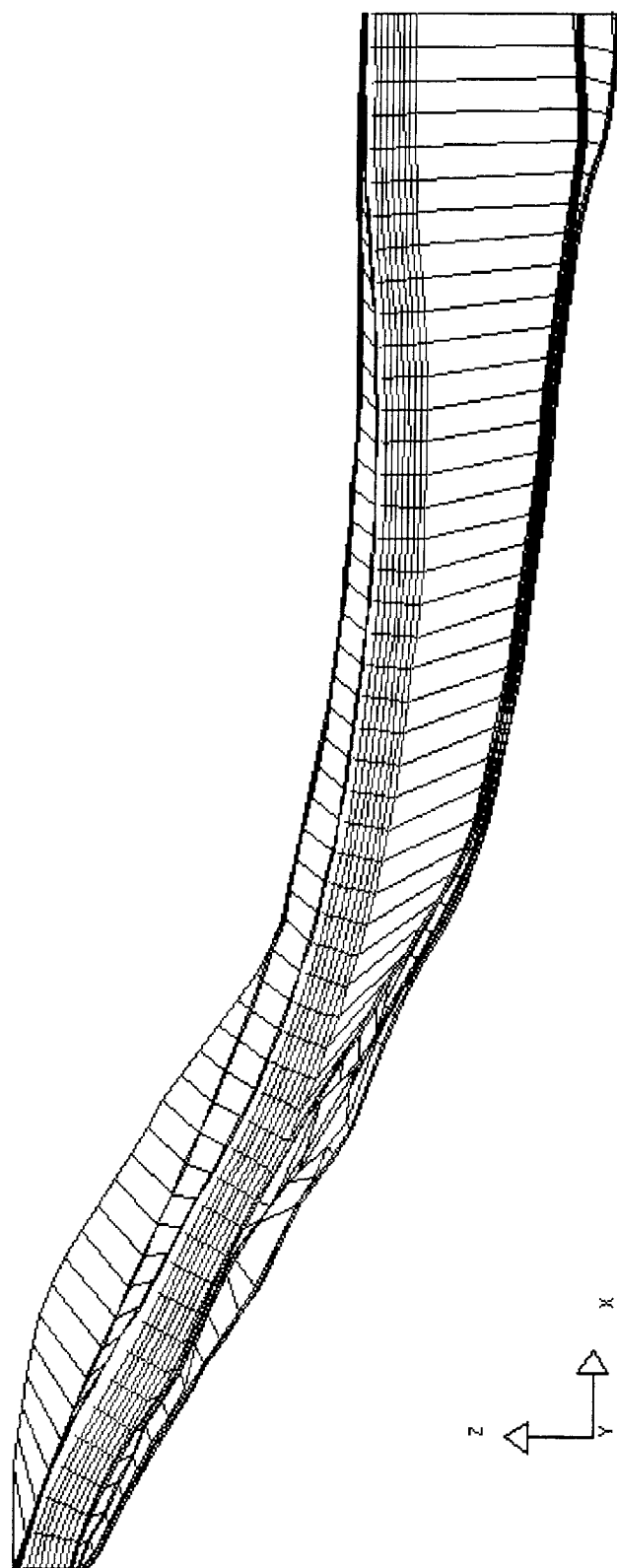
\* MAX. DISPL 9.87205E+001 AT NODE 102

CURRENT PART (P000001)

SCALE FACTOR = 1.000E+00

Figure 26. Response of a Half of Sandwich Panel with S2/Epoxy Face Sheets Subjected to Blast Load - Demonstration of Delamination Progression at 2.0 msec.

STEP 49 TIME = 2.400000E-003



\* MAX. DISPL 1.17791E+01 AT NODE 102

CURRENT PART (\*\*\*\*\*01)

SCALE FACTOR = 1.000E+00

Figure 27. Response of a Half of Sandwich Panel with S2/Epoxy Face Sheets Subjected to Blast Load - Demonstration of Delamination Progression at 2.45 msec.

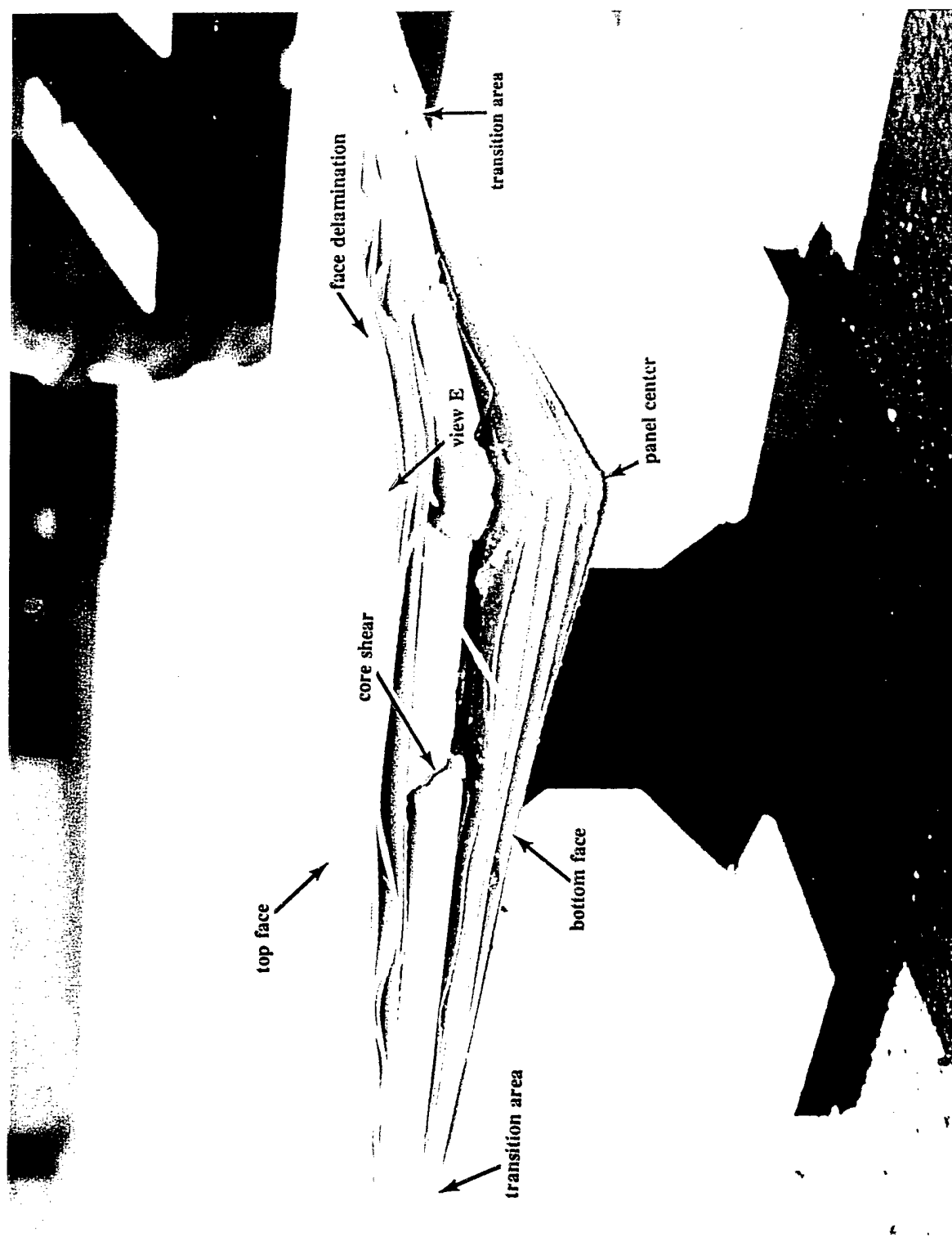
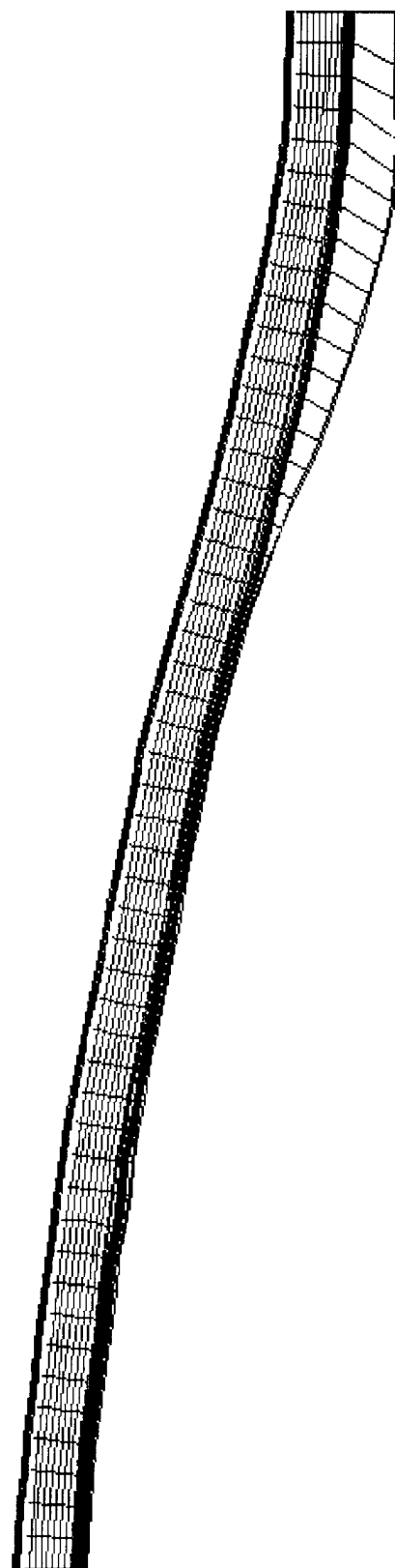


Figure 28. Extensive Delamination in Both Face Sheets is seen from the Sectioned Sandwich Panel after Mine-Blast Test ARL-TR-796 [22]



Z

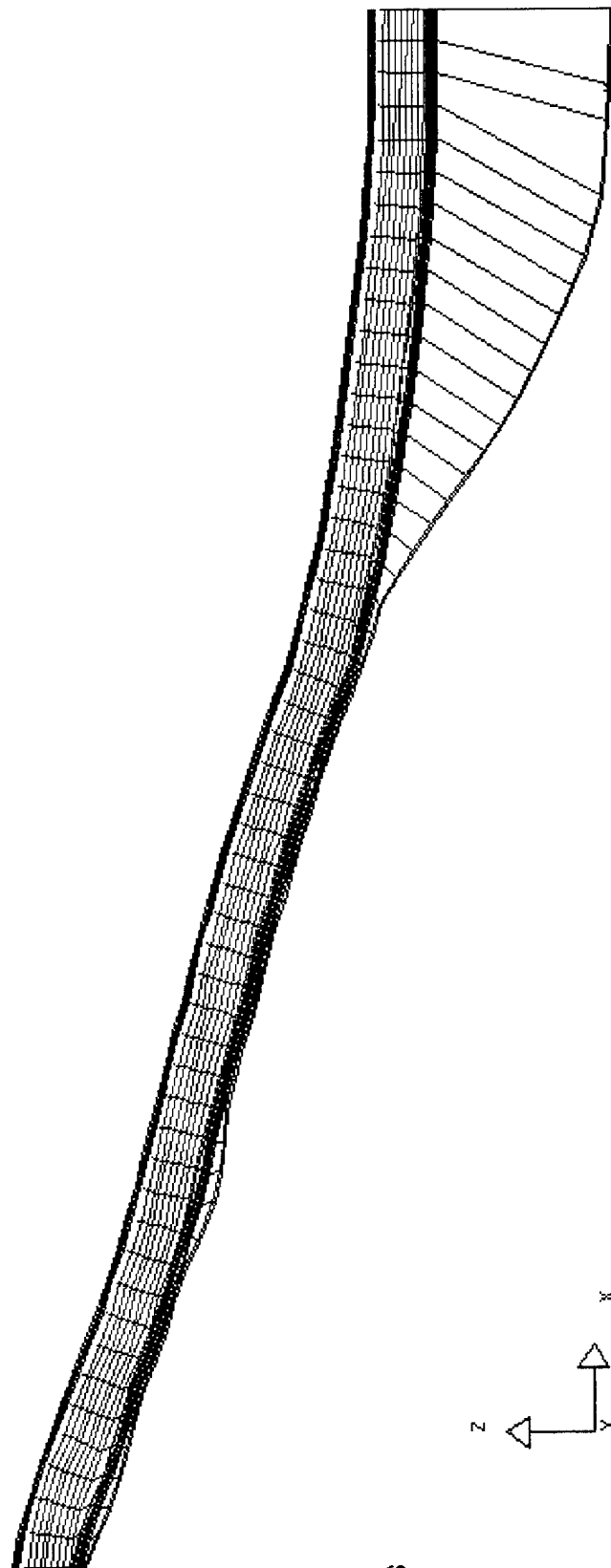
X

CURRENT PART [P000001]

Figure 30. Response of a Half of Sandwich Panel with IM7/Epoxy Face Sheets Subjected to Blast Load - Demonstration of Delamination Progression at 1.0 msec.



STEP 33 TIME = 1.6310100E-03



\* MAX. DISPL 1.23048E+01 AT NODE 99

CURRENT PART (\*\*\*\*\*1)

SCALE FACTOR = 1.000E+00

Figure 31. Response of a Half of Sandwich Panel with IM7/Epoxy Face Sheets Subjected to Blast Load - Demonstration of Delamination Progression at 1.63 msec.



## APPENDIX A

Suite 250, 500 Office Center Drive  
Fort Washington, PA 19034  
Tel: 215-542-8400 Fax: 215-542-8401

**25** Advanced  
Years Composites  
Technology

## APPENDIX A: AN EQUATION OF STATE FOR TRANSVERSELY ISOTROPIC MATERIALS

An equation of state that is suitable for a unidirectional composite material is derived in this Appendix. This generalized equation of state relates the pressure to both the volumetric strain and the deviatoric strain.

### Stress-Strain Relation

A typical unidirectional composite layer has isotropic properties in the plane transverse to fibers. Let axis number 1 designate the axis of symmetry (fiber direction). The stress-strain relations for a transversely isotropic material can then be written in the form

$$\begin{bmatrix} \sigma_{11} \\ \sigma_{22} \\ \sigma_{33} \\ \sigma_{12} \\ \sigma_{23} \\ \sigma_{31} \end{bmatrix} = \begin{bmatrix} C_{11} & C_{12} & C_{12} & & & \\ C_{12} & C_{22} & C_{23} & & & \\ C_{12} & C_{23} & C_{22} & & & \\ & & & 2C_{66} & & \\ & & & & C_{22} - C_{23} & \\ & & & & & 2C_{66} \end{bmatrix} \begin{bmatrix} \epsilon_{11} \\ \epsilon_{22} \\ \epsilon_{33} \\ \epsilon_{12} \\ \epsilon_{23} \\ \epsilon_{31} \end{bmatrix} \quad (\text{A1})$$

The five constants,  $C_{11}$ ,  $C_{12}$ ,  $C_{22}$ ,  $C_{23}$ , and  $C_{66}$  designate the five independent effective properties of the transversely isotropic medium. Those five elastic constants can be expressed in terms of the usual engineering properties as

$$\begin{aligned} C_{11} &= E_A + 4\nu_A^2 K_T \\ C_{12} &= 2K_T \nu_A \\ C_{22} &= G_T + K_T \\ C_{23} &= -G_T + K_T \\ C_{66} &= G_A \\ \frac{1}{2K_T} &= \frac{1 - \nu_T}{E_T} - \frac{2\nu_A^2}{E_A} \end{aligned} \quad (\text{A2})$$

where  $E_A$  is the axial modulus,  $E_T$  is the transverse modulus,  $\nu_A = -\epsilon_{22} / \epsilon_{11}$  is the axial Poisson's ratio,  $\nu_T = -\epsilon_{33} / \epsilon_{22}$  is the transverse Poisson's ratio,  $G_A$  is the axial shear modulus and  $G_T$  is the transverse shear modulus.

## Pressure - Strain Relation

The total stress,  $\sigma_{ij}$ , can be expressed as the sum of the deviatoric components,  $\sigma'_{ij}$ , and the pressure,  $p$ . That is

$$\sigma_{ij} = \sigma'_{ij} - \delta_{ij} p \quad (A3)$$

where  $\delta_{ij}$  is the Kronecker delta function and the pressure is defined as

$$p = -\frac{1}{3}(\sigma_{11} + \sigma_{22} + \sigma_{33}) \quad (A4)$$

The total strain,  $\varepsilon_{ij}$ , is related to the deviatoric strain,  $\varepsilon'_{ij}$ , and the volumetric strain,  $\Delta$ , as

$$\varepsilon_{ij} = \varepsilon'_{ij} + \frac{1}{3}\delta_{ij}\Delta \quad (A5)$$

Note that the volumetric strain is given by  $\Delta = V/V_0 - 1 = \rho_0/\rho - 1$  where  $V$  is the specific volume which is the inverse of density  $\rho$  and the initial values are denoted by the subscript "0". For small strain,

$$\Delta = \varepsilon_{11} + \varepsilon_{22} + \varepsilon_{33} \quad (A6)$$

and thus

$$\varepsilon'_{11} + \varepsilon'_{22} + \varepsilon'_{33} = 0 \quad (A7)$$

Substituting Equation (A5) into Equation (1), the pressure of Equation (A4) is

$$p = -\frac{1}{9}(C_{11} + 2C_{22} + 4C_{12} + 2C_{23})\Delta - \frac{1}{3}(C_{11} + 2C_{12})\varepsilon'_{11} - \frac{1}{3}(C_{22} + C_{12} + C_{23})(\varepsilon'_{22} + \varepsilon'_{33}) \quad (A8)$$

It is seen from Equation (A8) that for transversely isotropic materials, the pressure depends on both the volumetric strain and the deviatoric strain components.

For an isotropic material, the elastic modulus,  $E$ , and Poisson's ratio,  $\nu$ , are identical in all the directions. Utilizing Equation (A7), Equation (A8) for isotropic conditions reduces to:

$$p = -\frac{E}{3(1-2\nu)}\Delta = -K\Delta \quad (A9)$$

Equation (A9) is the usual expression for isotropic material that relates the pressure to the volume strain through the bulk modulus,  $K$ .

## Equation of State

## Equation of State

In LS-DYNA3D, a polynomial equation of state, which is linear in internal energy,  $E_g$ , is given as

$$p = C_0 + C_1\mu + C_3\mu^2 + C_4\mu^3 + (C_4 + C_5\mu + C_6\mu^2)E_g \quad (\text{A10})$$

where  $\mu = \rho / \rho_0 - 1 = -\rho\Delta / \rho_0$ , and the  $C_i$ 's are to be determined from experimental data. It is noted from Equation (A8) that the complete equation of state for transversely isotropic materials must account for the portion of pressure resulting from the deviatoric strain. Consequently, the equation of state of Equation (A10) is modified as:

$$p = C_0 + C_1\mu + C_3\mu^2 + C_4\mu^3 + (C_4 + C_5\mu + C_6\mu^2)E_g - \frac{1}{3}(C_{11} + C_{12})\varepsilon'_{11} - \frac{2}{3}(C_{22} + C_{12} + C_{23})(\varepsilon'_{22} + \varepsilon'_{33}) \quad (\text{A11})$$

The material constant  $C_1$  can be obtain from Equation (8). At small volumetric strain,  $\mu \approx \Delta$ . Therefore,

$$C_1 = -\frac{1}{9}(C_{11} + 2C_{22} + 4C_{12} + 2C_{23}) \quad (\text{A12})$$

For isotropic conditions,  $C_1$  reduced to the material bulk modulus.

S



## APPENDIX B

## APPENDIX B: A MIXTURE THEORY FOR EQUATION OF STATE

In this Appendix, the simple mixture theory given by Torvik [10] is used to develop the effective equation of state for a unidirectional composite under shock compression.

Note that Torvik's theory predicted the pressure-density relationship across a shock for a homogeneous isotropic mixture based on the Hugoniot relationships of the constituents.

Following Reference [10], a general mixture theory for the density change will be presented for a mixture with  $n$  constituents. The resulting system will then be used to obtain the effective equation of state for a fiber-reinforced composite.

### A MIXTURE RULE FOR DENSITY CHANGE

The constituent densities are related to the overall composite density as

$$\bar{\rho} = \sum_i v_i \rho_i \quad (B1)$$

where  $\bar{\rho}$  is the density of the mixture as a whole,  $\rho_i$  is the density of the  $i$ th constituent, and  $v_i$  is the volume fraction of the  $i$ th constituent. Since the partial mass density of the  $i$ th constituent is  $v_i \rho_i$ , the mass fraction,  $\gamma_i$  is defined as:

$$\gamma_i = \frac{v_i \rho_i}{\bar{\rho}} \quad (B2)$$

It is important to note that the mass fraction is constant for each constituent during shock deformation.

Rewriting equation (B1) in term of the mass fractions

$$\frac{1}{\bar{\rho}} = \sum_i \frac{\gamma_i}{\rho_i} \quad (B3)$$

Note that equation (B3) can be verified by using equation (B2).

After the material compression, the deformed density  $\bar{\rho}$  can be related to its value at the initial state as

$$\frac{\bar{\rho}_0}{\bar{\rho}} = \frac{\sum_i \frac{\gamma_i}{\rho_i}}{\sum_i \frac{\gamma_{i0}}{\rho_{i0}}} \quad (\text{B4})$$

where the subscript 0 refers to the initial (unstressed) state. Assume that the mass fraction remain constant during deformation, i.e.,  $\gamma_i = \gamma_{i0}$ , and realize that

$$\frac{\gamma_i}{\rho_i} = \frac{\gamma_i}{\rho_{i0}} \frac{\rho_{i0}}{\rho_i} \quad (\text{B5})$$

and

$$\frac{\frac{\gamma_i}{\rho_{i0}}}{\sum_i \frac{\gamma_i}{\rho_{i0}}} = v_i \quad (\text{B6})$$

Thus, equation (B4) can be rewritten

$$\frac{\bar{\rho}_0}{\bar{\rho}} = \sum_i v_i \left( \frac{\rho_{i0}}{\rho_i} \right) \quad (\text{B7})$$

The mixture rule of equation (B7) for density change was derived by Torvik. Similarly it can be readily shown that the following relation can be derived:

$$\frac{\bar{\rho}}{\bar{\rho}_0} = \sum_i v_i \left( \frac{\rho_i}{\rho_{i0}} \right) \quad (\text{B8})$$

Written in terms of the reduced density,  $\mu = \rho / \rho_0 - 1$ , the mixture rule has the form

$$\bar{\mu} = \sum_i v_i \mu_i \quad (\text{B9})$$

where  $\bar{\mu}$  and  $\mu_i$  are the reduced densities for the composite and the  $i$ th constituent, respectively. Equation (B9) will be used to obtain the composite equation of state in the next section.



## COMPOSITE EQUATION OF STATE

An approximate procedure will be introduced to obtain the effective equation of state for a unidirectional composite. This procedure can be readily extended to arbitrary laminate configurations.

In the monthly report of July, a polynomial equation of state with the generalization to transversely isotropic medium has been provided. It has the general form:

$$p = C_0 + C_1\mu + C_3\mu^2 + C_4\mu^3 + (C_4 + C_5\mu + C_6\mu^2)E_g - \frac{1}{3}(C_{11} + C_{12})\epsilon'_{11} - \frac{2}{3}(C_{22} + C_{12} + C_{23})(\epsilon'_{22} + \epsilon'_{33}) \quad (B10)$$

where  $E_g$  is the internal energy,  $C_{ij}$ , are the elastic constants given in July's monthly report. The material constant  $C_1$  is obtained in the small volumetric strain region,  $\mu \approx \Delta$  as,

$$C_1 = -\frac{1}{3}(C_{11} + 2C_{22} + 4C_{12} + 2C_{23}) \quad (B11)$$

Consider the equations of state for the fibers and the matrix in a unidirectional composite

$$p^m = C_1^m\mu^m + C_2^m\mu^{m2} + C_3^m\mu^{m3} + \Gamma^m E_g^m - \frac{1}{3}(C_{11}^m + C_{12}^m)\epsilon_{11}^{m'} - \frac{2}{3}(C_{22}^m + C_{12}^m + C_{23}^m)(\epsilon_{22}^{m'} + \epsilon_{33}^{m'}) \quad (B12)$$

and

$$p^f = C_1^f\mu^f + C_2^f\mu^{f2} + C_3^f\mu^{f3} + \Gamma^f E_g^f - \frac{1}{3}(C_{11}^f + C_{12}^f)\epsilon_{11}^{f'} - \frac{2}{3}(C_{22}^f + C_{12}^f + C_{23}^f)(\epsilon_{22}^{f'} + \epsilon_{33}^{f'}) \quad (B13)$$

where the superscripts f and m referred to the fiber and matrix, respectively. The same expression is used for the effective composite equation of state as

$$\bar{p} = C_1^c\mu^c + C_2^c\mu^{c2} + C_3^c\mu^{c3} + \Gamma^c E_g^c - \frac{1}{3}(C_{11}^c + C_{12}^c)\epsilon_{11}^{c'} - \frac{2}{3}(C_{22}^c + C_{12}^c + C_{23}^c)(\epsilon_{22}^{c'} + \epsilon_{33}^{c'}) \quad (B14)$$

where the superscripts c's are used to denote the corresponding composite values. The composite material parameters  $C_i^c$ ,  $\Gamma^c$  and  $C_{ij}^c$  will be obtained from the corresponding material parameters of fiber and matrix.

First, the composite elastic material parameters  $C_1^c$  and all the  $C_{ij}^c$  can be obtained at the elastic state (low pressure range) through an elastic micromechanical model such as composite cylinders assemblage. Next the composite Gruneisen constant  $\Gamma^c$  for the thermodynamic pressure will be obtained by assuming the overall requirement of partitioning the energy such that

$$\bar{\rho} E_g^c = \rho_m E_g^m + \rho_f E_g^f \quad (B15)$$

and the equilibrium of thermodynamic pressures in the constituents

$$\Gamma^m E_g^m = \Gamma^f E_g^f = \Gamma^c E_g^c \quad (B16)$$

Utilizing equations (B15) and (B16), we have

$$\frac{\bar{\rho}}{\Gamma^c} = \frac{\rho_m}{\Gamma^m} + \frac{\rho_f}{\Gamma^f} \quad (B17)$$

Finally, the material constants  $C_2^c$  and  $C_3^c$  will be obtained from the mixture rule for the reduced density of equation (B9) and the equilibrium assumption of the total pressure such that

$$\bar{p} = p^m = p^f \quad (B18)$$

At this moment, closed-form solutions are not available. However, at various pressure levels, the density changes in the fiber and matrix,  $\mu_f$  and  $\mu_m$ , respectively, can be computed from equations (B13) and (B14). By the use of equation (B9), a relation between the pressure and the composite reduced density  $\bar{\mu}$  can be established numerically. Through this relation, the constants  $C_2^c$  and  $C_3^c$  can be determined by the least squares curve fit. The only difficulty existing to implement this procedure is to evaluate the internal energies in the fibers and matrix at each pressure level. One approximation is to determine these two constants under isentropic low pressure rate condition where the thermodynamic pressure is negligible. The other alternative is to include the mixture procedure in the hydrocode where the internal energy of an element is available. Further evaluation concerning implementing the proposed mixture theory for the composite equation of state will be conducted in Phase II.



## APPENDIX C

Suite 250, 500 Office Center Drive  
Fort Washington, PA 19034  
Tel: 215-542-8400 Fax: 215-542-8401

**25** Advanced  
Years Composites  
Technology

## APPENDIX C: COMPOSITE LAYER FAILURE MODEL

Failure criteria utilizing all six components of stress will be incorporated in LS-DYNA3D to better characterize the damage in composite structures under mine blast loading. Hashin's failure criteria with a slight modification will be used to predict failure within a composite layer [8]. These criteria define distinct modes of failure for both the fiber and matrix. Under high compressive loading conditions, a Coulomb-Mohr type failure criterion recently developed at MSC, [9], will also be considered. All failure criteria are expressed in terms of stress components based on ply material coordinates  $(\sigma_1, \sigma_2, \sigma_3, \tau_{12}, \tau_{23}, \tau_{31})$  with 1 denoting the fiber direction.

### FIBER FAILURE MODES

The fiber tensile mode assumes a quadratic interaction between the axial stress and the maximum axial shear. The fiber tensile/shear failure is predicted when

$$\left[ \frac{\sigma_1}{S_1^t} \right]^2 + \frac{(\tau_{12}^2 + \tau_{31}^2)}{S_{12}^2} = 1 \quad (C1)$$

where  $S_1^t$  and  $S_{12}$  are the axial tensile and axial shear strengths, respectively. This criterion is applicable when  $\sigma_{11}$  is positive, and is used to predict a failure mode characterized by fiber breakage.

When  $\sigma_1$  is compressive it is assumed that failure is characterized by fiber buckling and is only dependent upon  $\sigma_1$ . The compressive fiber mode failure criterion is then given by the maximum stress criterion

$$\left[ \frac{\sigma_1}{S_1^c} \right]^2 = 1 \quad (C2)$$

where  $S_1^c$  is the axial compressive strength of the ply.

## MATRIX FAILURE MODES

Matrix mode failure are characterized by cracks running parallel to the fibers. Failures are described as being tensile or compressive, depending upon the sign of the quantity  $(\sigma_2 + \sigma_3)$ . Both matrix mode failure criteria assume quadratic interactions between the transverse stresses (both in-plane,  $\sigma_2$ , and through the thickness,  $\sigma_3$ ), the maximum shear in the transverse plane, and the maximum axial shear.

When  $(\sigma_2 + \sigma_3)$  is positive, the tensile mode criterion is used. This criterion is given by

$$\left[ \frac{\sigma_2 + \sigma_3}{S'_s} \right]^2 + \frac{(\tau_{23}^2 - \sigma_2 \sigma_3)}{S_{23}^2} + \frac{(\tau_{12}^2 + \tau_{31}^2)}{S_{12}^2} = 1 \quad (C3)$$

where  $S'_s$  and  $S_{23}$  are the transverse tensile and transverse shear strengths.

For  $(\sigma_2 + \sigma_3)$  negative, the compressive failure criterion is given by

$$\frac{\left[ \frac{\sigma_2 - \sigma_3}{2} \right]^2 + \tau_{23}^2}{S_{23}^2} + \frac{(\tau_{12}^2 + \tau_{31}^2)}{S_{12}^2} = 1 \quad (C4)$$

which is a simple quadratic interaction between the maximum transverse and axial shear stresses. Failure predicted by this criterion will be referred to as shear failure.

## DELAMINATION MODES

A delamination is a crack which runs in the resin-rich area between plies with different fiber orientation. Delamination caused by transverse impact usually occurs after a threshold of energy has been reached. It has been observed that delamination only occurs in the presence of matrix cracks. Taking into consideration of the presence of a high through the thickness normal stress due to the transverse blast wave, a simple strength criterion for delamination is assumed to have the following form.

For a tensile through the thickness normal stress,  $\sigma_3 > 0$ , the criterion is given by

$$S \left\{ \frac{\sigma_2^2 + \sigma_3^2}{S_2^2} + \frac{\tau_{23}^2}{S_{23}^2} + \frac{(\tau_{12}^2 + \tau_{31}^2)}{S_{12}^2} \right\} = 1 \quad (C5)$$

For a compressive through the thickness normal stress,  $\sigma_3 < 0$ , the criterion is given by

$$S \left\{ \frac{\sigma_2^2}{S_2^2} + \frac{\tau_{23}^2}{S_{23}^2} + \frac{(\tau_{12}^2 + \tau_{31}^2)}{S_{12}^2} \right\} = 1 \quad (C6)$$

Note that S is used as a scale factor which can be determined from fitting the analytical prediction to experimental data for the delamination area. It is also noted that the delamination criterion is provided as a first approximation for characterizing delamination progression under transverse blast loading conditions. For further study, it may be more appropriate to utilize a fracture mechanics delamination model, which is based on the critical values of interface energy release rates, to evaluate the dynamic delamination failure.